# The Cassini Magnetic Field Investigation — Source link

Michele K. Dougherty, S. Kellock, David J. Southwood, A. Balogh ...+9 more authors

**Institutions:** Imperial College London, California Institute of Technology, Braunschweig University of Technology, University of California, Los Angeles ...+1 more institutions

**Topics:** Magnetosphere of Saturn, Exploration of Saturn, Magnetosphere of Jupiter, Titan (rocket family) and Magnetosphere

Related papers:

- Cassini plasma spectrometer investigation

- The Cassini Radio and Plasma Wave Investigation

- Magnetosphere Imaging Instrument (MIMI) on the Cassini Mission to Saturn/Titan

- Cassini magnetometer observations during Saturn orbit insertion.

- A new form of Saturn's magnetopause using a dynamic pressure balance model, based on in situ, multi-instrument Cassini measurements

# THE CASSINI MAGNETIC FIELD INVESTIGATION

M. K. DOUGHERTY[1,*], S. KELLOCK[1], D. J. SOUTHWOOD[1], A. BALOGH[1],
E. J. SMITH[2], B. T. TSURUTANI[2], B. GERLACH[3], K. -H. GLASSMEIER[3],
F. GLEIM[3], C. T. RUSSELL[4], G. ERDOS[5], F. M. NEUBAUER[6], S. W. H. COWLEY[7]

[1]*The Blackett Laboratory, Imperial College London, SW7 2BZ, U.K.*
[2]*Jet Propulsion Laboratory, California Institute of Technology, Pasadena, CA 91109, U.S.A.*
[3]*Technische Universitat Braunschweig, D-38106 Braunschweig, Germany*
[4]*UCLA Institute of Geophysics and Planetary Physics, Los Angeles, CA 90024-1567, U.S.A.*
[5]*KFKI Research Institute for Particle and Nuclear Physics, PO Box 49, H-1525 Budapest, Hungary*
[6]*Institute for Geophysics and Meterology, Köln University, 50923 Köln, Germany*
[7]*Department of Physics and Astronomy, Leicester University, Leicester, LE1 7RH, U.K.*
(*Author for correspondence: e-mail: m.dougherty@imperial.ac.uk)

**Abstract.** The dual technique magnetometer system onboard the Cassini orbiter is described. This instrument consists of vector helium and fluxgate magnetometers with the capability to operate the helium device in a scalar mode. This special mode is used near the planet in order to determine with very high accuracy the interior field of the planet. The orbital mission will lead to a detailed understanding of the Saturn/Titan system including measurements of the planetary magnetosphere, and the interactions of Saturn with the solar wind, of Titan with its environments, and of the icy satellites within the magnetosphere.

**Keywords:** Cassini, magnetometer, saturn

## 1. Introduction

The ultimate goal of the Cassini–Huygens mission is a detailed understanding of the Saturn system with special emphasis on Titan. The Cassini orbiter provides extended monitoring of the Saturn system over a 4-year period resulting in a detailed description of the dominant physical processes and their variation with time, allowing separation of temporal and spatial features. In particular, repeated flybys of Titan provide a rather complete survey of the environment of this moon. The magnetometer in turn addresses the nature of the internal field, the planetary magnetosphere and its interaction with the solar wind, the magnetic states of the moons and how they interact within their plasma environments.

A magnetometer is an essential instrument for planetary studies and many different designs have been flown. The Cassini magnetometer has been designed and built specifically for measurements within the Saturnian environment. Previous planetary flybys have shown the existence of an internal Saturn magnetic field, a magnetosphere and a strong plasma interaction between Titan and its plasma surroundings. By measuring the planetary field and determining the relative size of

*Figure 1.* Schematic of Saturn's magnetosphere and magnetometer science objectives.

the major spherical harmonic components, which originate deep inside the planet the magnetometer will provide information on conditions in and near the dynamo region. However, the magnetometer probes not only the deep interior of the planet where the internal planetary field originates but also makes detailed measurements of the planetary environment, its magnetosphere and ionosphere, and of those of the Saturnian moons. This paper describes the science objectives of the magnetometer team, the instrument sensors and electronics, instrument calibration, data processing, as well as early cruise operations and the critical calibration data collected during the swingby past the Earth in August 1999.

The main scientific objectives of the Cassini magnetic field investigation are listed below as well as being shown schematically in Figure 1. They can be divided up into two main areas of research:

*Saturn*

- Resolve the internal planetary magnetic field to at least fourth order.
- Establish relative contributions to electromagnetic and mechanical stress balance.
- Identify the energy sources for dynamical processes.

- Understand the coupling that occurs between the magnetosphere and iono-sphere.
- Characterise the phenomena of the distant dayside/flank planetary environment.
- Survey satellite/dust/ring/torus electromagnetic interactions.
- Determine the tail structure and dynamic processes.
- Provide a three-dimensional global model of the magnetospheric magnetic field.

*Titan*

- Determine the magnetic state of the body and conditions of the atmosphere.
- Characterise and model the Titan electromagnetic environment.
- Interpret and model all Titan-plasma flow interactions and the variation of the Titan-magnetosphere interaction with respect to the Titan orbital phase.
- Determine the nature of the low frequency waves in the near-Titan plasma environment.

In addition the magnetic state and plasma environments of the Saturnian icy satellites will be probed to the extent possible within the limitations of the finally chosen tour.

The design of the instrument has been driven by a range of requirements; unique to a long-term interplanetary cruise, to the Cassini spacecraft and to the science goals listed above. The extremely long mission duration, from 1997 until at least 2008, requires high reliability and survivability. Due to the long delays in communication between the spacecraft and the ground, both the spacecraft and instruments must operate autonomously. To conform to practical limits on the use of the DSN network, the mission makes use of on-board data storage. The science aims require measurements with high sensitivity over a wide dynamic range (from tens of thousands of nanotesla (nT) during Earth flyby, through a few thousand nT expected during Saturn flybys to the extremely low field strengths in the solar wind). We have met these requirements with a novel instrument, a dual technique magnetometer (such as flown on Ulysses, Balogh *et al*., 1992) where we use vector helium (VHM) and fluxgate magnetometers (FGM) and also operate the helium device in a scalar mode (SHM). The instrument is capable of determining the *absolute* magnitude of the field to an accuracy of 1 nT. By calibrating FGM measurements with the absolute scalar measurements, determination of the fields in the Saturn environment will be possible with hitherto unachieved accuracy. The combination of V/SHM and FGM allows very sensitive determination of wave fields. The VHM is more sensitive below $\sim 1$ Hz, with the FGM being more sensitive at high frequencies. Simultaneous operation of both instruments will assure maximum sensitivity over the broad range of frequencies from 0 to 20 Hz. The Cassini mission will be the first time that the scalar magnetometer has been used on a planetary mission.

The instrument is a result of the co-operation and assistance of many people and science data analysis will involve many more. Team members are drawn from

Imperial College London (Imperial), Leicester University, Jet Propulsion Laboratory (JPL), University of California Los Angeles (UCLA), Boston University, Central Institute for Physics, Budapest (KFKI), Technical University of Braunschweig (TUB) and Köln University.

## 2. Science Objectives

Saturn's magnetosphere is one of the most interesting planetary plasma environments in the solar system sharing many of the characteristics of the magnetosphere of the Earth (solar wind dominated) and Jupiter (rotation dominated). In many respects, however, the Saturnian magnetosphere is unique due to the diversity of coupling mechanisms that exist between the various components of the Saturn system (such as the solar wind, Saturn's ionosphere, Titan, the icy satellites, the rings and the large clouds of dust and neutrals). Our existing knowledge of Saturn arises from the three planetary flybys (Pioneer 11 and Voyager 1 and 2), remote sensing observations and modeling work. This has allowed us to gain a preliminary understanding of the magnetic field, plasma, energetic particles, waves and auroral signatures. There remain a large number of unanswered questions with regards to our understanding of the Saturn environment, a number of which will be addressed in this paper. Probably one of the most remarkable and enigmatic issues, which remain is the high degree of axisymmetry of the Saturnian internal magnetic field, with its close alignment of dipole and rotation axes.

### 2.1. Interiors of Saturn, Titan and the Icy Satellites

The primary scientific objective of the magnetometer is a determination of the internal magnetic field of Saturn to at least the fourth order spherical harmonic terms. In addition a more complete characterization of the planetary field will be achieved and possible secular changes since the initial Pioneer and Voyager flybys will be investigated. Following the recent Galileo flybys of the Galilean moons which have revealed the existence of an internal field at Ganymede and induced magnetic fields at Europa and Callisto (see Section 2.1.2) the possibility cannot be ignored that Titan and some of the icy satellites may have internal/induced fields of their own. We describe the potential of the magnetic field investigation to probe the deep interior of Saturn and its satellites, thus enabling us, in effect, to "see inside" these planetary bodies. The Sun and most of the planets have large internal magnetic fields, which are being continuously generated by dynamo action deep in the interior of the planet as a result of highly conducting material which resides there. Dynamo action is known to generate magnetic fields at the different planets, for example, the magnetic field generated by the dynamos of the Earth and the Sun both reverse and the dipole axes for Uranus and Neptune are tilted by large angles away from their rotation axes. The best fit model for the Jupiter field, which is mainly that due to a dipole but with additional quadrupole and octupole terms

is tilted by $10°$ away from the rotation axis and when using a dipole model for the field results in an offset of the axis away from the planetary centre. For Saturn the surprising feature is that there is only less than $1°$ tilt between the rotation and dipole axes and the field shows a remarkable symmetry about the rotation axis.

### 2.1.1. *Saturn*

In situ measurements of the magnetic field of Saturn have been obtained from the three previous flyby missions, Pioneer 11 (1979) and Voyagers 1 and 2 (1980 and 1981), each of which consisted of a single flyby through the Saturnian environment. The Cassini mission as an orbiter, has an immense advantage over the previous flyby missions as regards the determination of the internal planetary field, since an orbiter provides a much more complete three-dimensional sampling of the magnetic field measurements over a wide range of latitudes, longitudes and radial distance. The internal field at Saturn is highly unusual, being highly axisymmetric with a close alignment between its dipole and rotational axes. However, auroral observations, periodicities seen in kilometric radiation and the formation of spokes in the B ring as well as energetic particles spectral modulation and spin periodicity observed in magnetic field observations (Carbary and Krimigis, 1982; Kaiser *et al.*, 1984; Grun *et al.*, 1992; Bhardwaj and Gladstone, 1982; Espinosa and Dougherty, 2000) suggest that longitudinal asymmetries do exist close to the planet.

In modelling the internal planetary field of a strongly magnetized planet it can be assumed to first order that outside the planet there are no significant sources and therefore the magnetic field can to a good approximation be derived from a scalar potential function, $B = -\nabla V$, where

$$V = a \sum_{n=1}^{\infty} \left(\frac{a}{r}\right)^{n+1} \sum_{m=0}^{n} P_n^m(\cos\theta) \left[g_n^m \cos(m\phi) + h_n^m \sin(m\phi)\right],$$

where $r$ is the distance to the planet's centre, $a$ is the planetary radius, $\theta$ and $\phi$ are the colatitude and east longitude, respectively, $P_n^m$ are associated Legendre functions with Schmidt normalisation and the $g_n^m$, $h_n^m$ (Schmidt coefficients) are internal field parameters. The Schmidt coefficients are chosen to minimise, in a least squares sense, the differences between the model field and the observed field. Field modelling at Saturn to date (Smith *et al.,* 1980a; Smith *et al.*, 1980b; Connerney et al., 1982; Acuna *et al.*, 1983; Davis and Smith, 1986, 1990) has revealed that the dipole is axially coincident with the rotation axis, with significant quadrupole and octupole terms. Taking the summation over n beyond the octupole ($n = 3$) term is unwarranted with existing data and the only significant model coefficients generated are those of $g_1^0$, $g_2^0$ and $g_3^0$, shown in Table I, in this instance for the SPV harmonic model (Davis and Smith, 1990), generated from magnetometer data from all three of the previous flyby data sets.

An important question is whether non-axisymmetric coefficients are present in the field and whether they can be inferred from more accurate measurements of the

TABLE I

Model coefficients for the SPV internal Saturn field

| $n$ | $m$ | $g_n^m$ | $h_n^m$ |
|---|---|---|---|
| 1 | 0 | 21,160 | |
| 1 | 1 | 0 | 0 |
| 2 | 0 | 1,560 | |
| 2 | 1 | 0 | 0 |
| 2 | 2 | 0 | 0 |
| 3 | 0 | 2,320 | |
| 3 | 1 | 0 | 0 |
| 3 | 2 | 0 | 0 |
| 3 | 3 | 0 | 0 |

magnetic field or will become evident in the higher degree terms. Suggestions put forward to explain this absence of non-axisymmetric terms include the possibility of a highly conducting shell outside of the dynamo region and rotating about Saturn's dipole axis (Stevenson, 1980) as well as the suggestion that the generation of the magnetic field has ceased at Saturn and that the higher order non-axial terms are decaying more rapidly than the axial lower order ones. The Cassini magnetometer has been designed specifically to detect these very weak higher order terms ($n > 3$) whose contributions outside the planet are significantly smaller than the lower order terms.

Extension of the spherical harmonic sequence describing the internal field above that of the dipole, quadrupole and octupole terms depends on the magnetometer being able to make very accurate measurements at low altitudes, inside of $4R_S$ over a wide range of latitudes and longitudes. Figure 2 (adapted from Connerney, 1993) reveals the close flyby trajectories of the previous spacecraft flybys past Saturn, that of Pioneer 11 and Voyagers 1 and 2, as a function of latitude and longitude. The radial distance of the spacecraft is also denoted at various intervals along the different trajectories. This figure clearly shows the very limited range of latitudes and longitudes at which the Saturn planetary field has already been measured for distances less than $4R_S$ and confirms how crucial measurements which Cassini will make inside of this distance will be (see Figure 3). To date inside of $4R_S$ there are only three short swaths of observations, for Pioneer 11 (periapse distance $1.3R_S$) over latitudes of $[\pm5°]$ and longitudes of $[135–190°]$; from Voyager 1 (periapse distance $3.1R_S$) over latitudes of $[-15°$ to $-35°]$ and longitudes of $[170–200°]$; and for Voyager 2 (periapse of $2.7R_S$) from latitudes $[-20–30°]$ and longitudes $[315–350°]$.

Table II predicts the expected size of the weak higher order coefficients which the magnetometer will need to measure in order to delineate the fourth and fifth

TABLE II

Expected internal field contributions at Cassini orbit

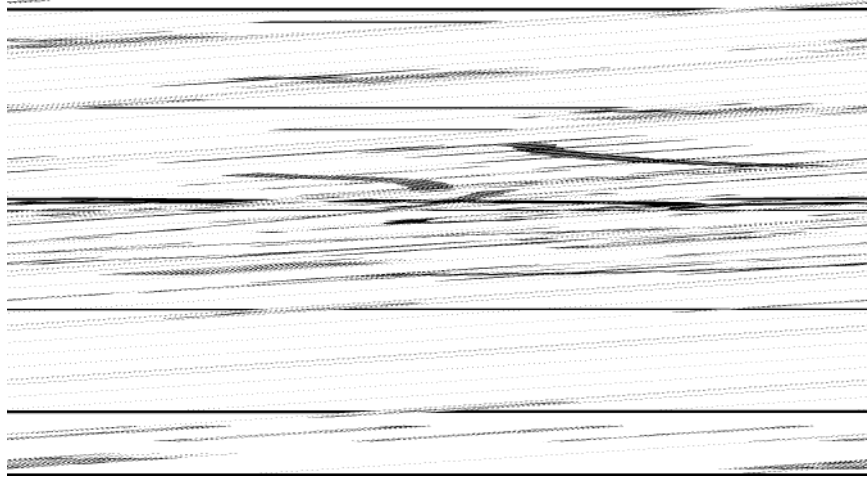| Harmonic Coefficient | Magnetic Field Magnitude at | | | | | |
|---|---|---|---|---|---|---|
|  | $1R_S$ | $1.5R_S$ | $2R_S$ | $2.5R_S$ | $3R_S$ | $4R_S$ |
| $g_1^0$ | 21,160 | 6,270 | 2,645 | 1,354 | 784 | 331 |
| $g_2^0$ | 1,560 | 308 (4.9%) | 98 (3.7%) | 40 (2.9%) | 19 (2.4%) | 6 (1.8%) |
| $g_3^0$ | 2,320 | 306 (4.9%) | 73 (2.6%) | 24 (1.8%) | 10 (1.3%) | 2 (0.6%) |
| $g_4^0$ | 2,000? | 176 (2.8%) | 31 (1.2%) | 8 (0.6%) | 3 (0.4%) | 0.5 (0.2%) |
| $g_5^0$ | 2,000? | 117 (1.9%) | 16 (0.6%) | 3 (0.2%) | 1 (0.1%) | 0.1 (0.03%) |



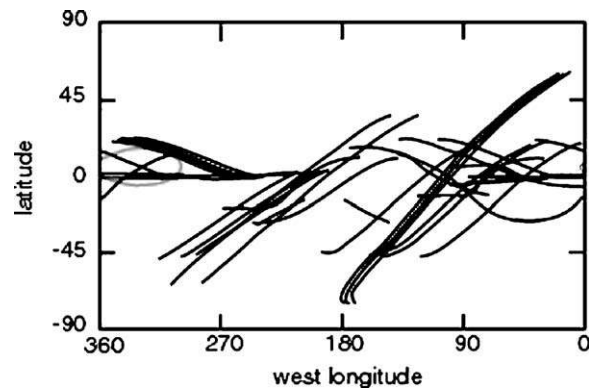*Figure 2.*  Close flyby trajectories of previous spacecraft.



*Figure 3.*  : Planned latitude and longitude coverage inside $4R_S$ by the Cassini spacecraft.

order components of the internal field. These values were estimated assuming that the higher degree terms were similar to the average of the quadrupole and octupole terms. If the field in the dynamo has equal power at all degrees as is true for the Earth (for example Elphic and Russell, 1978) these values will be somewhat reduced. These values stress how important the magnetic cleanliness of the Cassini spacecraft has been in order to carry out the science goals of the magnetometer as well as of the other fields and particles instruments, see Section 6. In addition the values in this table show how important data inside of $2.0R_S$ is for resolution of orders 4 and 5. The only time that this will occur is during Saturn Orbit Insertion confirming the criticality of magnetometer observations during this time for resolution of our prime science objective. The values shown in parentheses in Table II are the percentages of the total dipole field strength contributed by the coefficient at that distance.

Figure 3 shows the close flyby trajectories (inside of $4R_S$) of Cassini during the planned 4-year orbital tour, where ideally as much coverage of latitude and longitude space as possible is required in order to resolve the higher order moments.

It is the capability of the Cassini scalar magnetometer, which will be crucial to the high field operation of the instrument, with the scalar magnetometer allowing for precise absolute calibration of the fluxgate. In the past, a problem with achieving high accuracy from vector measurements has been the precise attitude knowledge required. For example, in a 10,000 nT field an accuracy of 1 nT in any component implies that the appropriate orientation angle must be known to within $10^{-4}$ or 20.6 arc sec. This can be achieved using special star trackers, for example, but with the SHM the problem is avoided by measuring the field magnitude directly by way of a resonance magnetometer. The fluxgate instrument, which has a large dynamic range has shortcomings in deriving accurate estimates of weak field components in a strong field. The vector helium magnetometer is able to make measurements of 1 part in $10^3$ at best for weak field components in a strong background field. However, on operating the helium magnetometer in its scalar mode and thereby directly measuring the Larmor frequency, measurements with an accuracy of 1 part in $10^5$ can be achieved. This improved accuracy of the SHM will allow measurements of the 4th and 5th order components of Saturn's internal field at distances further from the planet than those needed for the FGM. With the present mission profile, such an opportunity for the FGM would probably only occur at initial orbit insertion. SHM measurements can also be used to calibrate the analogue vector measurements to better than 1 part in $10^4$ (Langel *et al.*, 1981). Vector measurements in high fields near periapsis are critical in separating internal dynamo field components from externally generated magnetospheric currents.

### 2.1.2. *Titan and Icy Satellites*
The magnetic field measurements taken during the Galileo flybys of the Galilean moons revealed that Ganymede has its own internal field and that an electromagnetically induced magnetic fields arise at Europa and Callisto and possibly Ganymede due to currents on the conducting interior (assumed to be salty water) when the

external field changes as Jupiter rotates (Kivelson *et al.*, 1997; Kivelson *et al.*, 2000). The induced magnetic fields point to the probable existence of oceans below the icy crusts of these satellites (Neubauer, 1999; for a review see Kivelson *et al.*, 2002).

There are 44 close flybys of Titan planned during the 4-year orbital tour and the prime Titan-related science objective is to determine the internal magnetic field sources, be they from dynamo action, electromagnetic induction or remanent magnetisation in a "dirty ice" crust; as well as from sources external to it, such as ionospheric and plasma currents. Gaining an understanding of these sources will allow us to gain an understanding of the internal structure and evolution of Titan. The high sensitivity of the magnetometer instrument will ensure that Cassini will measure even a very weak internal Titan field to improve on upper limits and magnetic moments derived in the past (Neubauer *et al.*, 1984; Kabin *et al.*, 2000). The planned multiple flybys will allow measurements to be made at a range of latitudes, longitudes and altitudes enabling a better determination of an internal field to be made. If an internal ocean exists such studies will allow this to be probed.

In addition there will be 12 targeted (close) flybys of some of the icy satellites, including Phoebe, Mimas, Enceladus, Tethys, Dione, Rhea, Hyperion and Iapetus; as well as 28 untargeted (and therefore more distant) flybys as well. The science objectives arising from these flybys include the search for possible evidence of ancient dynamos and crustal remanence in the icy satellites as well as to investigate the icy satellite plasma environments (see Section 2.4). The study of any induced or intrinsic fields associated with satellites is important for a variety of reasons. It enables us to better understand the interior structure, composition and dynamics of the satellite, the way that particles from the magnetosphere impinge on the satellite and how this affects their evolution and the generation of magnetic fields in solid bodies in the solar system.

## 2.2. THE MAGNETOSPHERE

The Saturnian environment has to date been visited by three spacecraft, Pioneer 11 and Voyager 1 and 2. The trajectories of these spacecraft flybys are shown in Figure 4 (adapted from Sittler *et al.*, 1983) in a view projected onto the equatorial plane with approximate bow shock and magnetopause boundaries shown. In addition, the specific regions during which the spacecraft observed shock and magnetopause crossings is shown, clearly revealing the dynamic nature of the size of the magnetosphere. The limited spatial and local time coverage of the flybys is clearly evident.

### 2.2.1. *Electromagnetic and Mechanical Stress Balance*
Through much of the Saturnian magnetosphere the dynamics of the system are believed to be controlled by the rotation of the planet (McNutt, 1983), with the planet appearing to enforce corotation through much of the inner regions of the
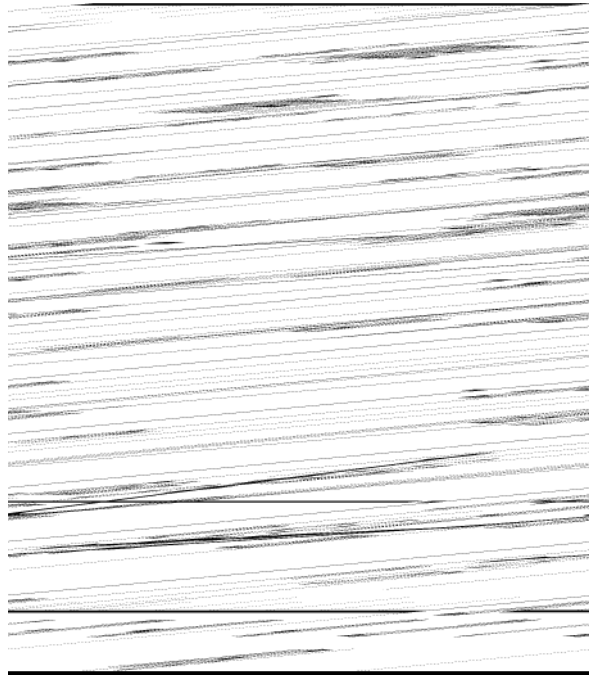
*Figure 4.* Equatorial view of the three spacecraft flybys of Saturn. On the trajectories the black dots labelled S show observed bow shock crossings, and black rectangles labelled M show observed magnetopause crossings.

magnetosphere. As material is ionised it is picked up in the corotational flow in the equatorial magnetospheric regions and rotational energy in the form of momentum is transferred from the planet to the equatorial plane. An unavoidable feature of any plasma which has been generated by ionisation where there is a background flow is that the thermal speed is at least comparable to the flow speed picked up. Separating the various forces exerted by the different parts of the particle distributions and by different species is a very important question and in a quasi-steady situation since all the mechanical forces are taken up by the magnetic field, the field is a natural area to study in order to aid the particle teams in this endeavour. A natural extension of the characterisation of the magnetospheric Saturnian field (see Section 2.2.7) would be to use the magnetic field data in conjunction with data from the other fields and particles instruments to examine the fundamental questions of what mechanical stresses the magnetic field stresses link to. The magnetic field imposes coherent behaviour on the collision free regions of the planetary environment and hence acts as the sinews of the medium. Stress is communicated by the field and energy is stored in the field and sometimes released by dramatic explosive phenomena like reconnection. Derived field and current patterns will aid in determining the balance of stresses and the relative importance of pressure and centrifugal forces.

### 2.2.2. *Energy Sources for Dynamical Magnetospheric Processes*

At the Earth it is clear that the dominant energy source for the magnetosphere is that due to the solar wind with the bulk of energy which drives magnetospheric dynamics arising from the coupling between the magnetosphere and the solar wind. At Jupiter, with its dominating internal plasma source Io, very fast rotation rate and very large magnetosphere, it is internal processes which are the dominant energy source, with the bulk of the magnetospheric energy being gained by transfer of the rotational energy from the planet out to the magnetosphere. At Saturn, although there can be no doubt that the outer Saturnian magnetosphere undergoes some form of dynamic interaction with the surrounding solar environment, the importance of energy transfer via the solar wind to the Saturnian system is, as a whole, thought to be of minor importance. The high rotation speed of the planet along with high corotation speeds imply that the centrifugal forces are very large in the outer magnetosphere and may alone dominate steady or sporadic transfer of material, momentum and energy between the planetary environment and the interplanetary medium. This question of which are the dominant processes governing plasma transport as well as the overall time variability of the Saturnian system will be addressed by the Cassini orbits of Saturn. We expect that in the inner magnetosphere, the dominant processes will be centrifugal in origin and hence plasma originating in the inner regions will undergo outward diffusion. Transport processes in the outer regions are more likely to be time dependent and are less well known. An important test of dynamical processes within the magnetosphere is being able to distinguish between the occurrence of substorms governed by solar wind behaviour or the periodic detachment of tubes of plasma being driven by planetary rotation or other time dependent effects.

A surprise discovery during the Ulysses flyby of Jupiter was the presence of what have been called null field events in the outer magnetosphere (Haynes *et al*., 1994). These nulls are sporadic drop-outs in field strength detected in the outer magnetosphere. It is believed that the spacecraft flew through regions of enhanced plasma pressure which were elongated along the ambient field direction. Following this discovery null fields were also found in all of the previous Jupiter flybys, that of Pioneer 10 and 11 and Voyagers 1 and 2 (Leamon *et al*., 1995). It has been proposed that these events are formed by the breaking off of material from the outer edge of the Jovian magnetodisk (Southwood *et al*., 1995). The plasma material is hence moving outwards and the nulls, therefore, play a role in the outward transport of iogenic material. At Saturn a number of similar types of field drop-outs with corresponding density enhancements have been observed, both inward and outward of the Titan orbit in the noon sector. In the Voyager 1 data they are seen on either side of the main Titan encounter plume and the observations are consistent with a general aging of the plume characterised by their dispersal by the centrifugal interchange instability. That is, there could be multiple encounters with an extended Titan plume, which has been wrapped around Saturn by corotation and could last for up to three Saturnian rotations before reaching background levels (Eviatar *et al*., 1982). In the Voyager 2 data density enhancements have been described as plasma blobs which have become

detached from the outer boundary of the nightside extended plasma sheet (Goertz, 1983). During the Voyager 2 flyby Titan was apparently in the magnetosheath or near the magnetopause boundary for a few days before the spacecraft entered the magnetosphere and hence one would not expect to see any plume evidence. The two theories, therefore, do not necessarily contradict one another. The Voyager 1 events translate to spatial dimensions of less than 1,600 km (or $0.027R_S$) if spacecraft motion alone is considered, whereas if it is assumed that the events are convected past the spacecraft at corotational speeds of order 150 km/s then the dimensions become 15,000 km (or $0.27R_S$). It is important to generate a consistent theory which explains these plasma blobs which have been observed on the dayside of fast rotating magnetospheres as well as ascertain whether such signatures are to be seen on the dusk or nightside of Saturn's magnetosphere. If it can be firmly established that the blobs are associated with the breaking away of material from the magnetodisk then the discovery will be important for the light it can throw on the nature of transport processes in the outer Saturnian magnetosphere and in fast rotating magnetospheres in general.

### 2.2.3. *Magnetosphere Ionosphere Coupling*

At Saturn it is the angular momentum arising from planetary rotation which is the main source of momentum input into the magnetospheric plasma. A central issue arising from this concerns the coupling of the planet's ionosphere to the magnetospheric medium by way of momentum and angular momentum transfer which takes place via field aligned currents. At Earth it is generally directed from the magnetospheric plasma to the ionospheric plasma, with the Earth gaining momentum from the solar wind. For Saturn, however, the flow is usually in the opposite sense with angular momentum being transferred from the ionospheric plasma to the magnetospheric plasma with the magnetosphere thereby gaining momentum from planetary rotation. Auroral emission is direct evidence of magnetosphere/ionosphere/atmosphere coupling which exists for a magnetised planet such as Saturn. The driving mechanism for such emission is charged particle precipitation along field lines. The association of auroral signatures with processes in the terrestrial and Jovian magnetosphere is well documented and accounts for a range of dynamical phenomena coupled via the magnetic field. Although many global properties of the Saturnian magnetosphere are different from those at the Earth and at Jupiter, the magnetic field undoubtedly plays a similar role in connecting magnetospheric processes with the auroral ionospheric events they trigger, and in particular in establishing large scale current systems closed in the ionosphere. There are a number of fundamental questions which remain unanswered about Saturn's aurora; are they due to electron or ion precipitation, are the precipitations due to wave-particle interactions and if so what type of waves are amplified and in what regions does this take place? Observations of Saturn in the near UV (220 nm) with the Faint Object Camera (FOC) on the Hubble Space Telescope (HST) have revealed a dark northern auroral oval (Ben-Jaffel *et al.*, 1995). Auroral

activity is usually characterised by light emitted around the poles of the planet. The dark oval observed at Saturn reveals that transport of energy and charged particles from the magnetosphere to the atmosphere of the planet at high latitudes induces auroral activity that not only produces auroral light but also UV dark material near the poles. The first bright aurorae at Saturn's northern and southern poles were observed in the far UV by the wide field planetary camera on HST. (See http://oposite.stsci.edu/pubinfo/pr/1998/05/index.html). These images allowed resolution of a luminous, circular band centred on the north pole where an enormous auroral curtain rose as high as 2,000 km above the cloud tops. Observations of magnetic field measurements in conjunction with observations from the Cassini optical remote sensing instruments during the Cassini orbits as well as with telescope viewing of the aurorae will be able to go a long way to answering some of the questions raised above.

### 2.2.4. *Characterisation of Phenomena in the Distant Dayside Planetary Environment*

Due to the orbiting nature of the Cassini mission as well as the rather elastic nature of the Saturnian magnetosphere, as evidenced by the range of dayside bow shock crossing distances observed by the previous Saturn missions of Pioneer 11, and the Voyager 1 and 2 spacecraft (Slavin *et al*., 1983), Cassini is expected to observe a large number of bow shock and magnetopause crossings over a range of local times. This region is the one which holds the key to the solar wind interaction with the planetary environment. In the most distant regime of the planetary environment, beyond the bow shock, upstream waves are generated on field lines which connect to the bow shock by ions which are reflected from the shock. This results in a complex foreshock region with the waves scattering the streaming particles and thereby reflecting and accelerating them. The Saturnian magnetosheath is known to be home to very large amplitude mirror mode waves (Tsurutani *et al*., 1982, 1993) such as have been observed at both the Earth and Jupiter. The characterisation of the sheath MHD wave spectrum will have important implications for the nature of the solar wind input into the planetary system. Detailed analysis of the magnetopause and its immediate environment is also important since it will enable one to determine whether the field penetrates through to the boundary, that is, whether the flux of the interior planetary field connects to the exterior solar wind field. This will answer the question as to whether solar wind activity directly controls internal magnetospheric activity. A full study of the magnetopause boundary crossings requires combining the field and plasma data to establish whether material is in fact crossing though the boundary and whether acceleration and heating are taking place. The boundary crossing is unlikely to be stationary with the motion being possibly caused by a variety of phenomena among which are: the steady reconnection process, sporadic reconnection, changes in solar wind pressure, Kelvin–Helmholtz instability and the centrifugally driven instability to name but a few. The wave modes and wave particle interactions in the regions both upstream and downstream of the bow shock will be

determined. The internal structure of the shock and magnetopause crossing will be examined as well as the occurrence of waves, reconnection and other phenomena at and near the magnetopause. The effect of internal magnetospheric rotation and external solar wind conditions on the shape and position of the magnetopause and bow shock will also be investigated.

### 2.2.5. *Survey Satellite Dust Ring Torus Electromagnetic Interactions*

The magnetosphere of Saturn has multiple internal plasma sources, with ionised material originating from the hydrogen torus, the Titan torus, Titan itself, the icy satellites, the planetary ionosphere and most uniquely from the rings of the planet. There is additionally the potential external source of the solar wind plasma. The dynamics of the magnetosphere as a whole and in particular that of the inner magnetosphere are controlled by the planetary rotation. As material is ionised within the magnetosphere, large amounts of rotational energy have to be transferred from the planet to the corotating plasma in the equatorial plane in order to bring the freshly ionised material up to corotation. This energy transfer takes place via the magnetic field which is effectively frozen into the flow. This energy and momentum is transferred via stress in the field by large scale field aligned currents which couple the planetary ionosphere and magnetosphere. These current systems generate an azimuthal field component which reverses across the equator and hence the existence of the current systems can be measured by perturbations in the $B_\phi$ field component. Departures from corotation have been measured at Saturn by the Voyager spacecraft (Richardson, 1986) and more recently by Ulysses at Jupiter (Dougherty *et al.*, 1993) where corresponding auroral signatures were also observed (Dougherty *et al.*, 1998). It is highly unlikely that the coupling between the planet and the newly ionised material occurs smoothly and this results in the presence of Alfvenic oscillations which, therefore, are a diagnostic of this coupling.

### 2.2.6. *Structure and Time Dependence of the Magnetotail*

One of the central issues to be addressed by the Cassini orbiter is the relative importance of solar wind stresses and planetary rotation stresses in determining the morphology of the near tail structure and, therefore, the overall dynamics of the outer magnetosphere. The time dependent studies made possible by Cassini will enable us to distinguish between substorm like processes, in which solar wind stress is released sporadically in an explosive manner or where centrifugally driven ballooning causes plasmoid formation (see plasma bubbles discussion in Section 2.2.2). From the Cassini magnetometer measurements we will be able to characterise the configuration of the Saturnian magnetic tail in the near planetary environment in terms of lobe field strength, orientation and variations, as well as properties of the magnetic field in the central plasma sheet. One will be able to, in conjunction with particle and plasma measurements, identify the relative contributions of rotational, pressure and field stresses to stress balance and thus determine which are the dominant processes.
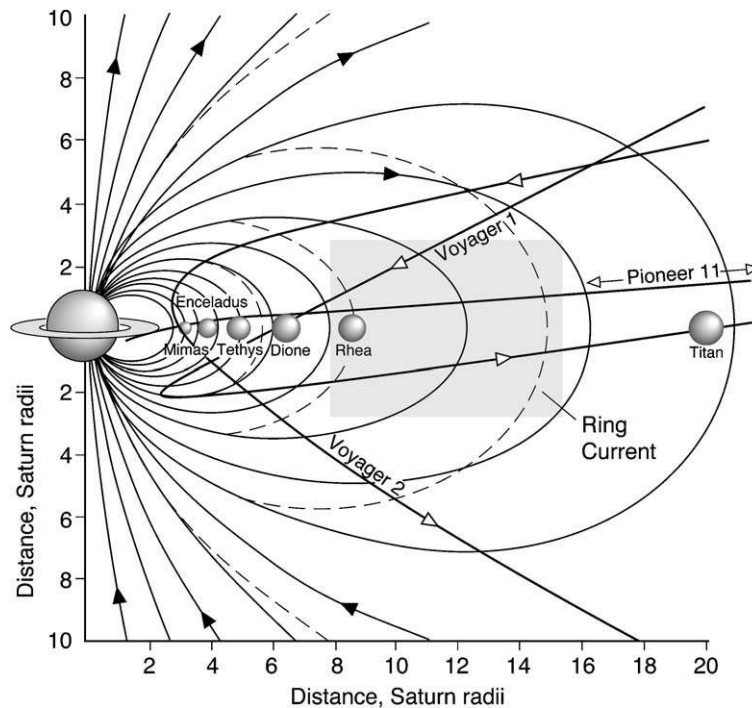
*Figure 5.* Meridional view of the modelled Saturn magnetic field showing the flyby trajectories overlain.

### 2.2.7. *Three-Dimensional Magnetospheric Field Model*

Figure 5 shows a meridional view of the modelled magnetic field lines (solid line) at Saturn (adapted from Connerney *et al.*, 1983; Blanc *et al.*, 2002). In the middle magnetosphere the dashed lines denote field lines due to the internal field alone, and the solid lines are those resulting from a combination of both internal field and the effect due to the ring current (which is assumed to flow in the shaded box, azimuthally around the planet). One can see that although the radial stretching of the field lines is clearly evident in this region, this effect is moderate compared to that at Jupiter. Also shown in figure 5 are the trajectories of the three planetary flybys and hence the latitudinal coverage achieved can clearly be seen.

The total magnetic field at Saturn consists not only of the internal planetary field, but also of the sum of contributions from a variety of external sources. For example, the equatorial ring current, magnetopause and magnetotail currents all generate magnetic fields which have an effect on the overall field. The modelling of the external field provides a means of encapsulating the field measurements on a global magnetospheric scale. It allows the magnetic field morphology of the Saturnian system to be concisely defined and will allow extrapolation of the field outside of the region of space which will be explored by the Cassini spacecraft.

The dominant external field component is that due to the equatorial ring current which results from the requirement that the centripetal acceleration which is associated with planetary rotation must be balanced by an electromagnetic $J \times B$ force, as well as from pressure gradient effects. These currents then distend the mainly dipolar field in the radial direction. The azimuthal equatorial ring current at Saturn has until now been modelled in a very similar way to the Jovian magnetodisk model (Connerney *et al.*, 1983). This ring current is represented by an annular disk extending from 8 to $15.5R_S$ in Saturn's equatorial plane. The current is assumed to be uniformly distributed in $z$ throughout the total disk of thickness $6R_S$ and decreases inversely with radial distance. This model is a crude representation of the Saturnian plasma sheet with the sharp edges of the sheet and the purely radial fall off of current with distance being the major weaknesses. This is, however, the model which has generally been used in recent research into Saturnian physics although improvements to this model are being sought (Bunce and Cowley, 2002; Giampieri and Dougherty, 2002). There are a number of models which have been generated for the Jovian and terrestrial magnetodisks which describe the physical conditions which arise there in a far superior way. We plan to consider, in collaboration with Cassini particle instrument teams, such alternate approaches at Saturn in order to generate a more physically valid magnetodisk model. Three of these approaches are: (1) A self-consistent model of the magnetodisk including centrifugal force and pressure effects (Caudal, 1986); (2) Analytical models which allow for modelling of current disks of finite thickness flanked by current free regions (Tsyganenko and Peredo, 1994); (3) A model using the Euler potential approach (Khurana, 1997) which allows the model to incorporate the hinging and delay of the current sheet with radial distance, sweep-back of the field lines and have realistic azimuthal current density profiles within the magnetosphere.

The contribution to the magnetic field arising from magnetopause currents depends strongly on the characteristics of the solar wind interaction with the planet. It is the balance between the internal magnetic pressure and the dynamic pressure of the solar wind which establishes the outer shape of the magnetosphere. Since the magnetised solar wind does not penetrate into the magnetosphere, currents develop on the magnetopause surface, which in turn induce a contribution to the magnetic field. The only model available to date which models the interaction of the solar wind with the Saturnian magnetosphere has been developed by Maurice and Engle (1995). This computes the size and shape of the magnetopause as well as the additional contribution to the total field from the surface currents. This has been carried out for a few values of solar wind pressure and only one direction for the incident solar wind. Extensions to this type of model will allow scenarios to be generated for large variety of solar wind pressure values (as observed at Saturn) as well as a variety of incident solar wind geometries with large inclinations to the ring plane.

The magnetotail of Saturn has not yet been traversed by any of the previous spacecraft which have visited the Saturnian magnetosphere. The magnetotail region into which the field lines and plasma are able to expand as they rotate around the

planet is thought to be a very important region for energy transport processes within the magnetosphere. The only existing quantitative model of the magnetic tail region was proposed by Behannon *et al.* (1981) where cross-tail currents which extend from 16 to 100$R_S$ downtail along the Sun–Saturn line have been incorporated which close onto the magnetopause. One route which we plan to follow is to model the magnetotail contribution along the lines of a general Tsyganenko terrestrial model (Tsyganenko, 1989) to Saturn's dimensions. This model takes into account the effect of warping of the tail current in two dimensions. Any models generated will naturally depend on the physical measurements and processes which are observed during the Cassini orbits.

## 2.3. TITAN

Following the recent orbits of the Galileo spacecraft past the Galilean satellites of Io, Ganymede, Europa and Callisto with their measured internal/induced fields—there is now a renewed interest in the history and evolution of such moons. This holds not only for Jovian satellites but also for the Saturnian moons with the upcoming Cassini observations. The possibility of an internal/induced magnetic field at Titan is discussed in Section 2.1.2 as are the measurements which the Cassini orbiter will be able to make in this regard. Other Titan-related science targets of the Cassini orbiter are described briefly below.

### 2.3.1. *Empirical Model of the Titan Magnetoplasma Environment*

Titan has by far the densest atmosphere of any known satellite and is the second largest satellite in the solar system (with Ganymede being the largest). It is at a radial distance of 20$R_S$ from Saturn and although it spends most of the time within the Saturnian magnetosphere there are times when the solar wind pressure is high enough such that Titan can in fact be outside of the Saturnian bow shock or magnetopause (as probably occurred during the Voyager 2 flyby in 1981; Sittler *et al.*, 1983). Another interesting effect which occurs at Saturn is that there are periods when the planet is located within the Jovian magnetotail. It seems very likely that this occurred during the Voyager 2 flyby past Saturn (Lepping *et al.*, 1983). Depending on its position within the Saturnian environment, Titan constitutes an obstacle to the magnetospheric, magnetosheath or solar wind flow. Following the Voyager 1 pass through the wake of Titan, it is known that a strong interaction occurs with a magnetotail configuration (reviewed in Neubauer *et al.*, 1984) and an associated plasma cavity (Keller *et al.*, 1994). The implications of the relatively small scale size of Titan in relation to the Larmor radius of the upstream ions implies that serious asymmetries could result from the interaction. During the numerous Titan flybys which will take place during the Cassini mission, a description of the Titan environment which quantifies the structures detected in the vicinity of the body will be derived utilising the magnetic field measurements. Examples of such structures are: the size and shape of the magnetic cavity, size and opening angle of

the magnetotail, width of the plasma sheet and mantle and critical parameters for any Alfven wing-like structures and wave phenomena in its environment. A bow shock might be observed when Titan is in the solar wind.

2.3.2. *Titan-Plasma Flow Interactions and Variations of Titan/Magnetosphere Interaction with Respect to Titan's Orbital Phase*
As discussed in Section 2.3.1 the Titan orbit can, depending on solar wind conditions, be either inside or outside of the Saturnian magnetosphere. During the periods when Titan is inside of the magnetosphere, encounters will take place at a variety of phases of the Titan orbit, resulting in large stress variations between Titan and the surrounding plasma. Such stresses will be revealed by perturbations in the magnetic field measurements in the vicinity of the moon. Near the noon meridian, exits into the magnetosheath and the solar wind are also possible depending on solar wind conditions at the time. All such encounters will be documented and compared with theoretical models. As Titan orbits Saturn, the angle between the corotational flow and the direction of the ionising solar photons varies through $360°$. This leads to a variety of interesting cases at different local times which may prove to be important for the diagnostics of the plasma physical processes of the Titan interaction. For example, around Saturnian local time (LT) 06:00 hours induction effects should be most visible, around (LT) of 18:00 hours the cumulative action of solar photoionization and collisional ionization by magnetospheric electrons will lead to the strongest interaction.

## 2.4. ICY SATELLITES ELECTROMAGNETIC ENVIRONMENT

As described in Section 2.1.2, there will be numerous targeted and untargeted flybys of the icy satellites during the 4-year Cassini orbital tour. In addition to the search for internal/induced magnetic fields at these moons we will also investigate the icy satellite plasma environments. This will allow us to understand the electromagnetic interaction which arises between the various satellites and their surrounding plasma medium, whether it be Saturnian plasma or solar wind plasma. Here, the inner satellites seem to be particularly promising with Enceladus and the E-ring being prominent.

## 2.5. NATURE OF THE LOW FREQUENCY WAVE SPECTRUM

For a multi-ion plasma, such as found in the vicinity of Titan and the other icy satellites, even the presence of small concentrations of heavy ions greatly modifies the properties of the waves. In particular, new critical frequencies are introduced, in the form of resonance and cut-off frequencies (Dougherty and Southwood, 1993; Thompson *et al.*, 1995). Resonant frequencies are important since they reveal the frequency at the boundary of a stop band and in warm plasma theory wave particle

interactions occur close to resonant frequencies. The cut-off frequencies separate frequency bands of propagation to ones of evanescence. An additional critical frequency which arises in a multi-ion plasma is that of the cross-over frequency at which the phase velocity of right and left hand circularly polarised waves is the same as that of the transverse mode and in the vicinity of the proton Alfven speed. Since the new critical frequencies depend not only on the gyro-frequencies of each species present but also on the relative abundances of each, this implies that by careful interpretation of the frequency spectrum information can be obtained on which species are present as well as on the relative abundances of these species. Ion cyclotron wave activity at Jupiter has recently been examined in both the Ulysses (Dougherty *et al.*, 1997) and Galileo (Huddleston *et al.*, 1997) magnetic field data sets and observations of such wave activity were observed inside Saturn's magnetosphere by the Pioneer 11 spacecraft (Smith and Tsurutani, 1983). Work on the Galileo Io observations (Huddleston *et al.*, 1998; Huddleston *et al.*, 1999) compares pick-up processes near Io to those in the solar wind as well as showing the wave spectra can be used to infer plasma composition.

There are in fact a number of reasons for interest in ion cyclotron wave activity. Not only can they be used as a diagnostic as to what type of ion species arise in a plasma, but they can also be used as a means of coupling different species via wave particle interactions. Some ultra-low frequency (ULF) pulsations are standing MHD waves in the Earth's magnetosphere, with there being indications that such eigen-oscillations may also exist at Jupiter and Mercury although none have been observed in the Saturnian magnetosphere. Work by Cramm *et al.*, 1998 shows that the Voyager 1 spacecraft crossed an area of resonant mode coupling during its Saturn encounter. The sensitivity and high time resolution of the magnetometer will enable us in conjunction with the Cassini radio wave instrument to better resolve the wave spectrum at Saturn, for example, very close to the planet only the magnetometer has the capability of resolving down to the proton gyro-frequency.

### 3. Instrument Details

The chosen instrument configuration consists of a fluxgate magnetometer (FGM) and a vector helium magnetometer capable of operating in scalar mode (V/SHM). The instrument is intended to measure small changes in fields spanning four orders of magnitude with extremely high sensitivity. This is achieved in part by mounting the sensors on an 11 m spacecraft boom, the V/SHM at the end of the boom, the FGM halfway along it. The magnetometer boom distances the sensors from the stray magnetic field associated with the spacecraft and its subsystems and especially with spacecraft generated field variations, spacing the sensors at different distances along the boom allows this field to be better characterised and removed from the observations. The efforts taken to constrain the stray spacecraft field are described very briefly in Section 6. Sensitivity is also enhanced by the use of 16 bit analogue-digital converters (with 14 bit values being sent to ground). Mounting the sensors on

a boom could result in their orientation with respect to the spacecraft axes changing from time to time, after spacecraft manoeuvres for example. A means of sensor alignment determination has been provided by the Cassini project; the Science Calibration Subsystem, SCAS. This consists of two, perpendicular, coils rigidly mounted on the spacecraft body with a known alignment to the spacecraft axes. These produce well-defined magnetic fields on command which can be detected by the sensors and used to correct for any changes in sensor orientation. SCAS measurements taken to date will be described in Section 4.2.

What are the scientific advantages of the FGM, VHM combination and the scalar mode (SHM)? Both magnetometers are well capable of measuring the magnetic field vector at the location of the respective sensor at rates from DC up to 10 Hz (VHM) or at least 30 Hz (FGM). The VHM optimises low frequency vector measurements in low fields, FGM measurements are best at high frequency and it operates over an extremely wide dynamic range from very low fields ranging up to measurements in Earth's high field. The particular advantages of joint FGM, SHM measurements have been discussed in Section 2.1.1. The twin sensor configuration also contributes to overall instrument reliability; if one sensor fails field measurements can be made with the other sensor, with sufficient performance to achieve many of the major objectives of the investigation. Reliability has been further increased by the provision of redundant instrument power supplies and data processing units and by careful selection of electronic components which can survive the radiation environments encountered during the long cruise phase of the mission and in the Saturnian system. The VHM provides the stability needed to maintain the calibrations obtained in the solar wind while Cassini is inside the Saturnian magnetosphere for long periods during the 4-year tour.

An implicit feature of scalar or resonance magnetometers are null zones which arise if the ambient field falls outside a cone of $45°$ half angle with respect to the optical axis of the magnetometer. This results in the signal being dramatically weakened and hence the absolute accuracy of the instrument will suffer. As a result of use of the scalar magnetometer on Cassini, a requirement has been placed on the mission to avoid spacecraft orientations inside of $4R_S$ which cause the planetary field to lie within the null zones of the scalar device. This results in the signal being weakened with an associated decrease in absolute accuracy.

Other features of the instrument which have been driven by the characteristics of the mission and by the design of the spacecraft are to be found in the data processing unit (DPU). This contains a bus interface unit (BIU) provided by the Cassini project for interfacing to the onboard data handling subsystem (CDS) bus. In line with the spacecraft design, the DPU is capable of handling Packet Telemetry and Telecommands and features a flexible telemetry storage and generation scheme to support the multiple telemetry modes of the spacecraft. The tour operations concept requires that the DPU is able to handle trigger commands which initiate multiple actions within the instrument (macro commanding). Further, in order to optimise the analysis of discrete events such as shock crossings, a snapshot capability has

been implemented by which up to 16 Mbytes of data can be stored for later downlink at higher time resolution than normal. This capability can be initiated by command or triggered by pre-defined events.

Magnetic field information is needed by other investigations on the spacecraft. To this end magnetic field data are made available to onboard users every second. These onboard ancillary data are raw, uncalibrated vectors, the data source being selectable by command between the two sensors.

In total, the instrument consists of the two, boom-mounted, sensors, subchassis No. 1 (an assembly containing electronics for the FGM, VHM and SHM, the heater control electronics, the power supplies and power management system) and subchassis No. 2 (an assembly containing the data processing unit). Both subchassis are mounted in bay 4 of the Orbiter upper equipment module (UEM). Figure 6 shows the location of the magnetometer hardware on the spacecraft together with the spacecraft and sensor axes. An overall block diagram of the instrument showing how the hardware responsibilities for the individual elements have been divided between Imperial, JPL and TUB is shown in Figure 7. The instrument ground support equipment was provided by KFKI and TUB.

Table III lists the main characteristics of the instrument. Power and data rate values vary according to instrument mode. The values given are for the delivered flight model where power values include power drawn by the Cassini-provided BIU.

## 3.1. THE FGM

The FGM sensor is mounted halfway along the magnetometer boom, its associated analog electronics form part of the electronics assembly on Subchassis No. 1. A cable of approximately 6.5 m length runs along the boom between sensor and electronics. A high efficiency, tuned drive design of the electronics has been chosen to reduce power consumption and the effect of cable loading.

The FGM is similar to the Imperial instrument flown on Ulysses and to many others flown on numerous missions. It is based on three single-axis ring core flux-gate sensors mounted orthogonally on a machinable glass ceramic block. Ceramic is chosen for its low thermal expansion coefficient, minimising misalignments between sensors due to temperature changes. In each sensor, a drive coil is wound around a high permeability ring core which is completely enclosed in a sense winding. The drive coil is driven by a crystal-controlled 15.625 kHz square wave which is used to generate a magnetic field driving the core into saturation twice per cycle. The three drive coils are connected in series to simplify the cabling and circuitry. The presence of an ambient magnetic field component parallel to the axis of the sense coil causes the saturation of the core to become asymmetrical. This induces a second harmonic of the drive frequency in the sense coil which is proportional to the magnitude of the magnetic field component along that axis. The signal is processed through a narrow band amplifier tuned to the second harmonic of the
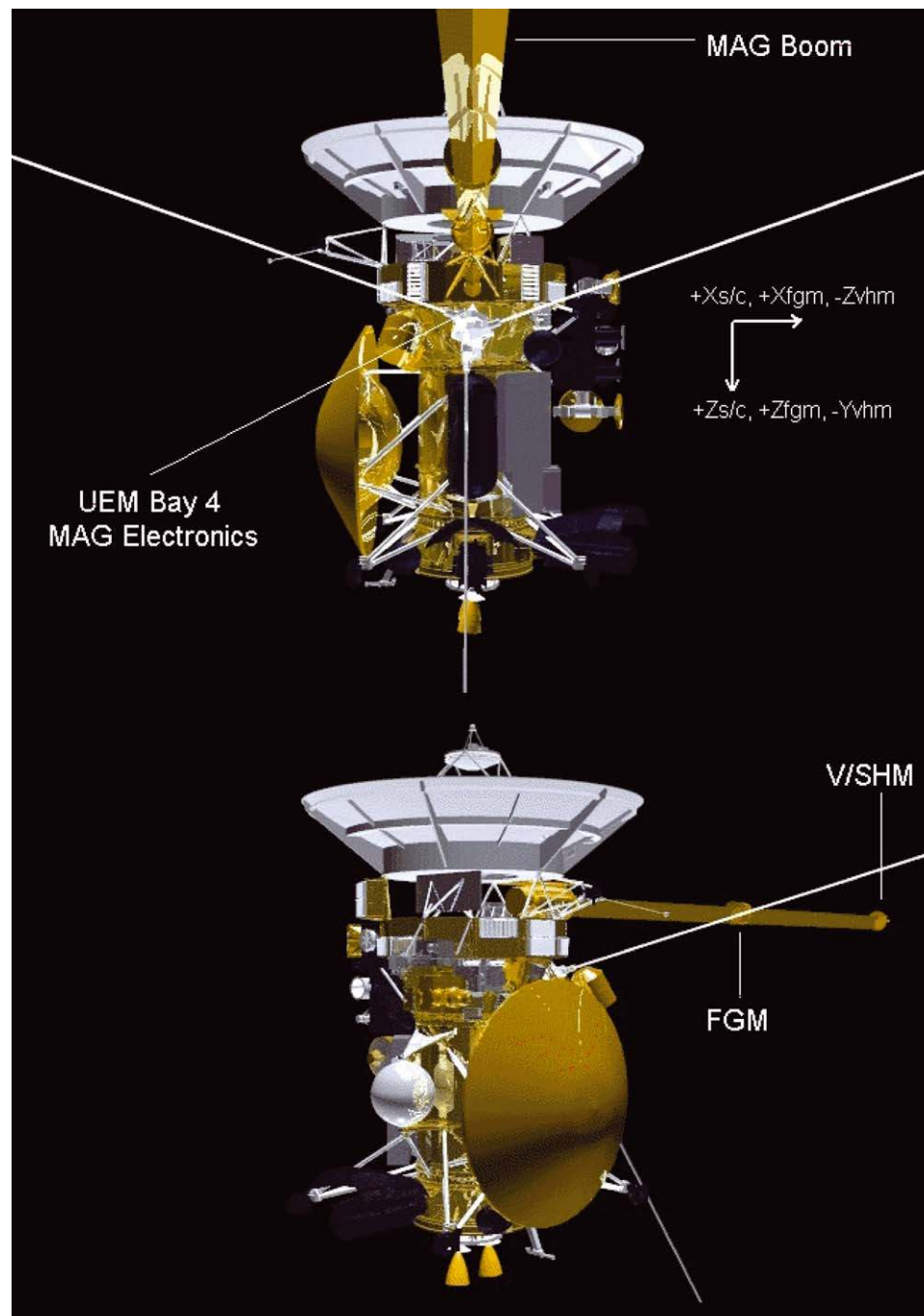
*Figure 6.* The placement of magnetometer hardware on the spacecraft is shown as well as the axes of the sensors (source: JPL).

*Figure 7.* Overall block diagram of the magnetometer instrument which also shows the institutes responsible for hardware. Command and data interfaces are shown as dotted lines and power interfaces are shown by solid lines.

drive frequency, which attenuates harmonics other than the second. The result is integrated, converted to a current and fed back to the sensor coil to null the ambient field. The integrated output voltage, amplified and corrected for scale factor and alignment errors, is proportional to the ambient field. The three analogue vector components are passed to the DPU for analogue to digital conversion and data processing. The noise performance of the FGM, measured on ground at the analogue output of the electronics, is better than 5 pT/$\sqrt{\text{Hz}}$ at 1 Hz. The electronics can be checked in flight using an in-flight calibration (IFC) capability built into the electronics and controlled by command from the DPU. The IFC applies a fixed offset to each of the three vector outputs corresponding to a signal of approximately 10 nT. The frequency, number of on/off cycles, of the IFC is selectable by command.

Changing the electronics feedback path and the output amplification allows the sensor to be operated in one of four different full scale magnetic field ranges, as listed in Table III. The largest range ($\pm 44{,}000$ nT) was included mainly for ground testing in the Earth's field. Switching between ranges in normal operations is automatic, controlled by the DPU. The DPU monitors each FGM component field value, if the magnitude of any of these exceeds an upper threshold for greater than a specified number of samples, the DPU will switch the FGM to a higher range. Similarly, if all three component value magnitudes fall below a lower threshold for more than a specified number of samples, the DPU will switch the FGM to a lower range. All parameters are modifiable by command and autoranging can also be disabled and manual range changes commanded.

TABLE III

Main Instument Characteristics

| | |
|---|---|
| Mass (kg) | |
| V/SHM Sensor | 0.71 |
| FGM Sensor | 0.44 |
| Subchassis#1 (Power Supplies, Sensor Electronics) | 5.15 |
| Subchassis#2 (DPU) | 2.52 |
| Total | 8.82 |
| Power (W) | |
| Sleep Mode | 7.50 |
| Vector/Vector Mode (FGM+VHM) | 11.31 |
| Vector/Scalar Mode (FGM+SHM) | 12.63 |
| Normal downlink data rate | |
| FGM | 32 vectors/s |
| VHM | 2 vectors/s |
| SHM | 1 value/s |
| Housekeeping | 24 bits/s |
| Total | 2,000 bits/s |
| Dynamic range, resolution | |
| FGM | $\pm$40 nT, 4.9 pT |
| | $\pm$400 nT, 48.8 pT |
| | $\pm$10,000 nT, 1.2 nT |
| | $\pm$44,000 nT, 5.4 nT |
| VHM | $\pm$32 nT, 3.9 p |
| | $\pm$256 nT, 31.2 pT |
| SHM | 256 –16384 nT, 36 pT |

A 1 W heater has been provided to maintain the FGM within its operating temperature range of $-30$ to $+50\,^{\circ}$C. The specially designed, non-magnetic unit is mounted on the ceramic sensor block and has control electronics on Subchassis No. 1. Further thermal control is provided by an aluminised mylar covered fibreglass case over the sensor block and by three, project-provided, radioactive heater units mounted equidistant around the sensor base (the latter provide a total of 3 W). Figure 8 is a photograph of the Fluxgate sensor, with its case removed showing the location of the single-axis sensors on the sensor block, together with its associated electronics.

## 3.2. THE V/SHM

The V/SHM sensor is mounted at the end of the 11 meter magnetometer boom. A photograph of the V/SHM sensor and the VHM electronics is shown in Figure 9.
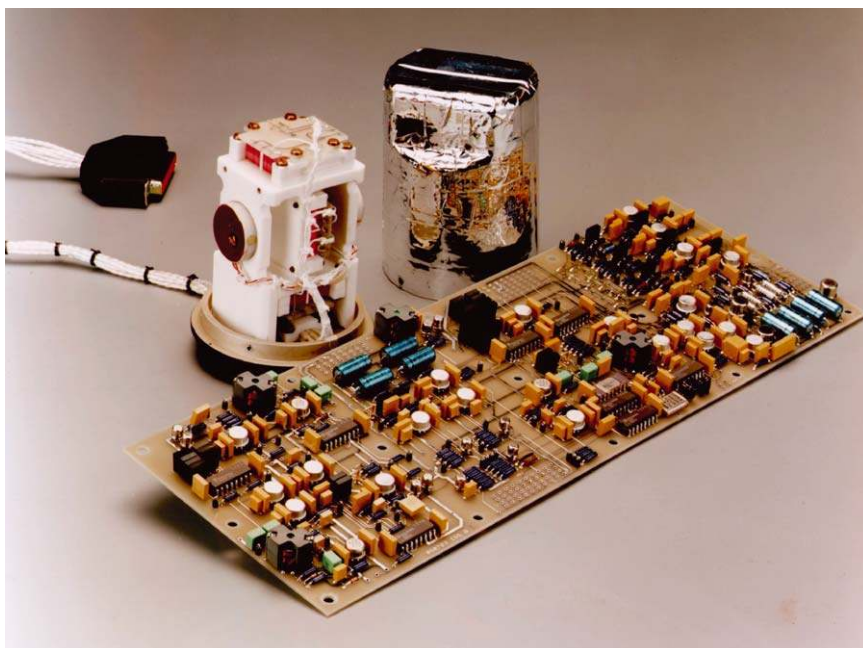
*Figure 8.* Ultra Electronics photograph of the FGM (with cover off) and electronics board.
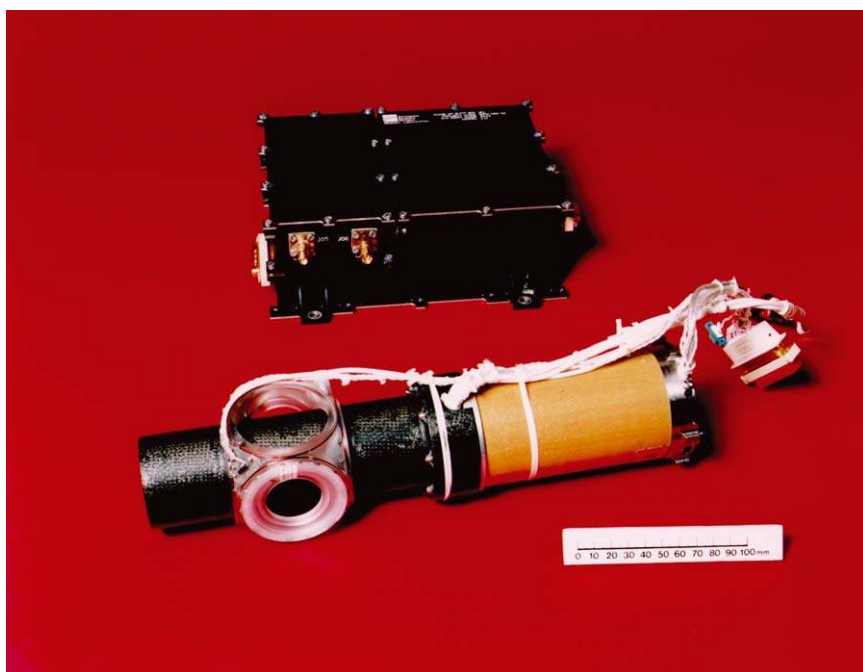


*Figure 9.* V/SHM sensor and VHM electronics.

A set of cables running the length of the boom connect it to the VHM and SHM electronics on Subchassis No. 1. The flight sensor is actually the flight spare Ulysses vector helium magnetometer sensor with the addition of a small pair of coils nested inside a pair of the larger Helmholtz coils used in the vector mode and a coaxial cable carrying the signal from the voltage controlled oscillator (VCO) to that cable. Similarly, the VHM electronics box is the Ulysses flight spare unit with small modifications to change the sensor operating ranges and to compensate for the different boom cable lengths. A new electronics board has been added to Subchassis No. 1 containing the electronics to operate in the scalar mode.

The operation of the magnetometer is based on field dependent light absorption (the Zeeman effect) and optical pumping to sense the magnetic field. Helium in an absorption cell is excited by a radio frequency (RF) discharge to maintain a population of metastable long-lived atoms. Infrared radiation at 1083 nm from a helium lamp, also generated by RF excitation, passes through a circular polariser and the cell to an infrared detector. The absorption (pumping efficiency) of the helium in the cell is dependent on the ambient magnetic field direction. The optical pumping efficiency is proportional to $\cos^2\Theta$ where $\Theta$ is the angle between the optical axis and the direction of the magnetic field. This directional dependence is utilised in the vector mode by applying low frequency sweep fields rotating about the cell, which allow the extraction of the three orthogonal ambient field components. These fields are fedback using a set of triaxial Helmholtz coil mounted on the sensor housing around the cell. In the scalar mode, the directional dependence results in a "field of view" restricted to a cone with half angle approximately $45°$, centred on the optical axis detector.

Changing the VHM sweep fields allows the sensor to operate in different ranges. Two VHM ranges have been selected for Cassini (see Table III). As for the FGM, automatic ranging has been implemented in the DPU. The VHM electronics also have an internal autoranging capability (used for the Ulysses instrument). A single range has been implemented for the SHM. Injection of known currents into the Helmholtz coil system provide an in-flight calibration (IFC) capability. The calibration fields apply an offset of approximately 1/8 of the full scale range to each vector component. A non-magnetic proportional heater using up to 2 W is incorporated into the V/SHM sensor and is controlled from electronics built into the VHM electronics box on Subchassis No. 1. The operating temperature range of the sensor is $-10$ to $+40\,°\text{C}$.

In the scalar mode, a weak AC field at the Larmor frequency is applied to the cell, which opposes the optical pumping. The decrease is detected by the IR detector as a decrease in transmitted light from the lamp. The Larmor frequency which is proportional to the ambient magnetic field is measured. In order to track the ambient field the applied field is frequency modulated so that the detector output contains a signal component harmonically related to the modulation frequency. The
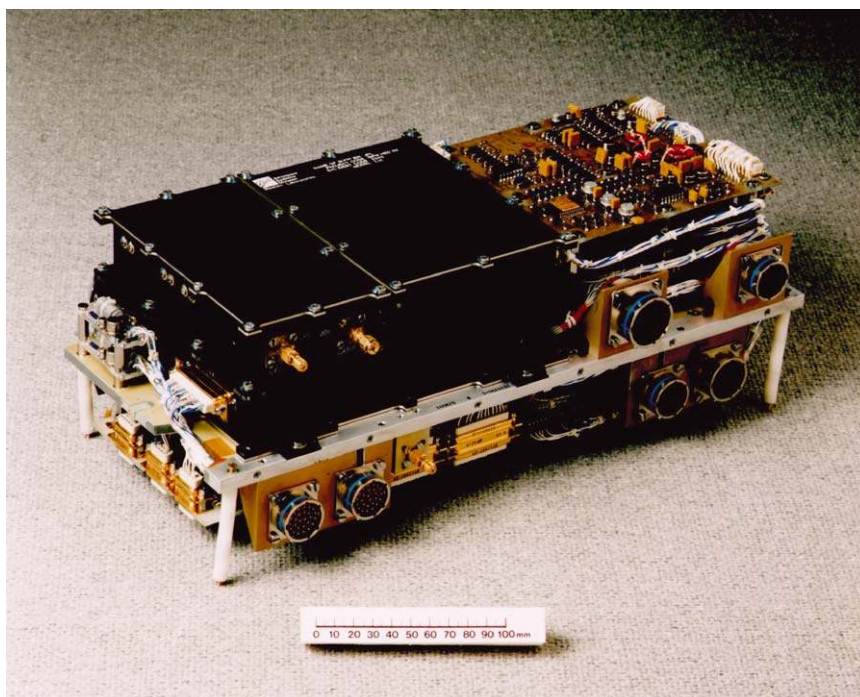
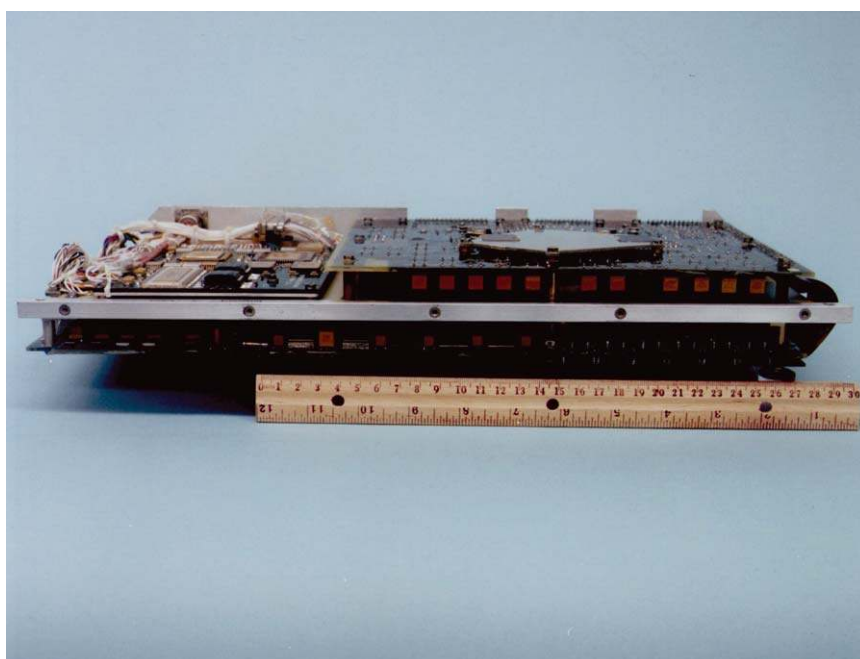*Figure 10.* Photograph of Subchassis No. 1 with the VHM sensor on top.



*Figure 11.* A photograph of Subchassis No. 2.

proportionality constant is the gyromagnetic ratio which for helium is 28.023561 Hz/nT. Detection and measurement of the Larmor frequency lead to a very accurate measurement of the ambient field magnitude. The result is passed as a 20 bit scalar word from the SHM electronics to the DPU. A more detailed description of the V/SHM may be found in Kellock *et al*. (1996). Smith *et al*. (2002) provides a detailed description of the SHM operation and observations from the Earth swingby in August 1999.

### 3.3. INSTRUMENT ELECTRONICS

The instrument electronics are all mounted in Upper Equipment Module bay 4 (see Figure 6) and are split between two subchassis assemblies. Subchassis No. 1 contains all the sensor electronics, the power supplies and power management system as well as the heater control and instrument housekeeping electronics. Figure 10 is a photograph of the Subchassis No. 1 assembly, its mass is given in Table III. On the underside of the subchassis, as seen from the photograph, are from the bottom upwards, the power management board, the FGM electronics board and the SHM electronics board (shielded from the other electronics by a grounded plate). The power management board contains a total of 14 non-latching power switches and cross-strapping circuitry for the two redundant secondary power supplies. The top side of the subchassis contains the black VHM electronics box (a modified spare unit from Ulysses), two small boards to the left of the VHM box with latching relays to switch between VHM and SHM operation, two redundant, secondary power supplies (PSU1 and PSU2), a dedicated BIU power supply (PSU0) and the top board contains the FGM heater control electronics and housekeeping circuitry. Proportional control electronics for the VHM heater are located within the VHM box. The power supplies and switches are Imperial designs used on previous missions and feature built-in overcurrent trips.

The basic power distribution scheme is described in Kellock *et al*., 1996. Power switches for the secondary voltage lines are controlled by the active processing unit and power switches for the power supplies and processing units themselves are controlled by discrete commanding from the spacecraft via the BIU and the Common Core (CC).

Subchassis No. 2 contains the DPU, consisting of two redundant processor systems plus a small CC and the BIU. When power is first supplied from the spacecraft, only the BIU and the CC become active, powered from PSU0. The BIU allows data transfer to and from the spacecraft, the CC processes commands and data for power up of the secondary power supplies (PSU1 or PSU2) and the processors (PUA or PUB). Each processor system is based on an 80C86 processor with 4 MHz clock, 32 kByte PROM, 128 kByte Hi-Rel RAM and 16 MByte state-of-the-art commercial DRAM. The systems normally operate singly but can be operated in parallel. A high accuracy 16 bit analogue to digital converter (ADC) is

integrated into each processor system for sensor data collection. Two ADC clock speeds are available; 1 and 2 MHz, the former being the default. Tantalum shielding has been used for the ADCs, DRAMs and Operational Amplifiers to reduce their susceptibility to radiation. The assembled subchassis is shown in Figure 11. The DPU boards are folded around the subchassis. The electronic components face to the subchassis, because the 2.4 mm thick 16-layer boards provide additional radiation shielding. The Sensor Interface Board is on the right hand side. The outer side shielding of the ADCs and Operational Amplifiers can be seen. The flexible connection board goes through subchassis cutouts to the Processor Board on the other side. The JPL-provided BIU plus its associated cabling is located on the left side.

To satisfy the demands of a deep-space mission with limited communications, the DPU has been designed with a large measure of autonomy and sophisticated data handling functions. The functions it performs are as follows: telecommand handling, sensor autoranging and IFC, sensor data collection, sensor data processing, snapshot data handling, telemetry generation, error correction, fault detection and recovery, and onboard ancillary data generation. Autoranging and IFC have been discussed above; data functions are described in the data processing Section 7. The remaining functions are briefly described below.

The DPU is designed to handle both the packet telecommand standard adopted by Cassini, used for normal commanding, and discrete telecommands used when the processor is not active. A large variety of command functions are supported which are discussed later. The DPU must be able to accept telecommands at all times, in all operational modes. Commands may be for immediate execution, or can contain relative or absolute timetags for delayed execution (relative timetags cause execution at a fixed time with respect to reception of the command, absolute timetags cause execution at specific spacecraft times). As noted earlier, a macro commanding capability has been implemented whereby sequences of instrument commands can be stored in the DPU and the sequence started by executing a macro command.

Hamming single bit error correction and double bit error detection is provided for all memory devices (except those in the BIU). Single Event Upsets (SEUs) can change the content of memory cells, cyclic access to every memory cell corrects single bit and reduces the risk of double bit errors. Memory scrubbing is initiated every 64 s in the Hi-Rel RAM and the 16 MByte, multi-snapshot, DRAM. It takes about 1 h to scrub the complete RAM. Additional memory checks can be initiated by command: occurences of single and double bit errors are monitored. The PROMS are checked separately and contain a pre-defined error pattern for detection. If a permanent RAM problem arises, the DPU can be commanded to run its software directly from PROM. In-flight tests have also been implemented for the ADC to check the noise and conversion and settling times on each analogue channel.

Both processor systems contain four separate dual level latch up detectors, one for the processor, one for the multi-snapshot memory and one each for the ADC $\pm 12$ V supply voltages. Detectors of similar design have been flown on the GEOTAIL, WIND and SOHO spacecraft. If a latch up is detected in the processor, it will be immediately switched off and on again and the instrument will be automatically reconfigured into its previous mode. Latch ups in either the memory or the ADC will cause it to be immediately switched off and back on again. There is also a hardware watchdog function in the DPU which will detect problems in the DPU program flow and which initiates a hardware reset followed by an automatic instrument reconfiguration.

The SCAS, provided by the Cassini project for alignment checks of the sensors on the magnetometer boom, consists of two coils, one (Y coil) located in UEM bay 4 and one (X coil) located in UEM bay 7. Its operational use is entirely under the control of the magnetometer team. The standard operational procedure is as follows: Upon electronics power up the SCAS $X$ coil is energised and operates for 34 min 8 s, swapping polarity every 2 s. After this SCAS automatically switches to the $Y$ coil which is operated in the same way. This cycle repeats until SCAS is powered off.

## 4. Calibration

Instrument calibration is an ongoing activity that begins at instrument assembly and continues throughout the mission. Before launch the sensors were calibrated in highly accurate test facilities; in-flight calibration signals have been regularly applied since launch; and the well characterized magnetic field of the Earth was used as a calibration source during Earth swingby.

### 4.1. GROUND CALIBRATION

#### 4.1.1. *Calibration of the Fluxgate Magnetometer*
The fluxgate magnetometer was calibrated in the 2.5 m Braunbek coil system of the Institute of Geophysics at the Technical University of Braunschweig (TUB) during the period June 24 to July 12, 1996. Tests were performed to calibrate the sensitivity (nT/bit), orthogonality, zero levels, linearity and frequency response. Functional tests of the auto-ranging, in-flight calibration and snapshot event trigger were also performed at this time. Detailed test procedures are documented in TUB reports CA-IGM-TP001 and test results in CA-IGM-TR-0002 and -0003. Key test data were reduced by two independent teams and then cross-checked. Table IV lists the sensitivities of each of the three sensors in each of the four ranges of operation of the magnetometer, normalised by the nominal range.

TABLE IV

Fluxgate magnetometer sensitivities

|  | | Output/Input | | |
| --- | --- | --- | --- | --- |
| Range (nT) | | X sensor | Y sensor | Z sensor |
| R0 | 40 | 0.9966 | 1.0002 | 0.9991 |
| R1 | 400 | 0.9994 | 0.9997 | 0.9997 |
| R2 | 10,000 | 0.99931 | 0.99952 | 0.99953 |
| R3 | 44,000 | 0.99938 | 0.99950 | 0.99950 |

TABLE V

Orthogonalisation matrices

| Range | Matrix |
| --- | --- |
| R2 | (1.0007 −0.00210 0.00304) (0.00202 1.0005 0.00159) (−0.00169 −0.00769 1.0005) |
| R3 | (1.0006 −0.00210 0.00302) (0.00205 1.0005 0.00161) (−0.00169 −0.00771 1.0005) |

Table V lists the matrices that convert the sensor measurements into a calibrated orthogonal field measurement. Both tables are for the sensor at room temperature. Only the matrices for the two highest field ranges are given here because the small size of the off-diagonal terms makes these elements difficult to determine in low field strengths. To a high degree of accuracy the corresponding matrices for the low field ranges can be obtained by replacing the diagonal terms in the R2 or R3 matrix by the reciprocal of the corresponding sensitivities in Table IV. Converting the off-diagonal terms to the equivalent angles between the sensors gives the following: XY angle, $89.998°$; XZ angle, $90.076°$ and YZ angle $89.650°$.

The frequency response of the basic (analog) fluxgate magnetometer is such as to have negligible impact on the instrument performance. The 5 dB point for the $X$ and $Z$ sensors is about 158 Hz and for $Y$ about 70 Hz. The phase lag is about $−100°$ at 200 Hz on all three sensors. The phase and amplitude response of the magnetometer in the final data stream will be set principally by the high rate sampling of the analog to digital converter (64 samples/s) and the averaging of the data processing unit (nominally 32 samples/s). The linearity test revealed the instrument to be extremely linear. The only non-linearity detected was at the level of $\pm 4 \times 10^{-5}$ of full scale in the x-sensor. This non-linearity appears to be sinusoidal and can be easily removed if necessary in data processing.

### 4.1.2. *Calibration of the V/SHM*

The calibration of the V/SHM in the vector mode was carried out at JPL in a magnetically-shielded walk-in room that contains a precisely calibrated set of Helmholtz coils. The sensor was mounted on a turntable whose angular position is controlled from outside the room. Means are available to vary the temperature of both the electronics and sensor independently. A standard comprehensive calibration procedure was followed that has been developed for past missions such as Ulysses. It involves accurate measurements of essentially all performance parameters including the triaxial scale factors (voltage out for a given field in) and linearity, intrinsic instrument noise, triaxial offsets (equivalent to the output in zero field), the amplitude and phase response as a function of frequency, response to the in-flight calibration signals (several positive and negative field steps applied to the sensor coils upon command), and orthogonality of the three axes.

Since the Cassini Flight Model is basically the Ulysses spare VHM built in the early 1980s, a long history exists consisting of calibration data taken at approximately 6 month intervals when the instrument was removed from JPL bonded stores for that purpose. Within the instrument field-equivalent-noise level (30 pT$^2$/Hz independent of frequency/white noise), no changes in any of the parameters with time or temperature have been detected. This stability has been confirmed in-flight by the Ulysses VHM over an interval of 12 years with accompanying excursions in temperature as the spacecraft traveled between 1 and 5.4 AU. In particular, any variation in magnetometer offsets is a few pT per year at most (and even this may be changes in spacecraft field).

Operation in the vector, and especially the scalar mode, was tested and calibrated at a coil facility maintained by the US Coast and Geodetic Survey magnetic observatory located outside Fredricksburg, Virginia. The SHM output was carefully compared with the fields produced by a set of large coils about 10 meters in diameter arranged in a Braunbek array that had previously been calibrated with a proton precession magnetometer. A high precision standard resistor was placed in series with the coils to monitor the coil currents very accurately. Close agreement was found between the SHM output and that based on the currents in the large coils and the corresponding calibration constants.

Special tests were run to measure small departures of the SHM output frequency from the true Larmor frequency having multiple causes. The sensor exhibits small vector offsets when operated in the scalar mode which had to be determined accurately so as to be able to remove them from the data if necessary. An additional small source of error that was measured accurately was the so-called "light shift" that arises because of the perturbation of the quantum energy levels by the incident radiation. Finally, at low fields (less than 1,000 nT), the Bloch-Siegert shift, whose magnitude depends on the ratio of the amplitude of the VCO-generated field to that of the ambient field, was characterized. The procedures used and the data taken have been documented in a test report and a final calibration report, the latter to provide the parameters need to reduce the V/SHM data to accurately known fields.

TABLE VI

Vector helium magnetometer sensitivities

| | Output/Input | | |
| --- | --- | --- | --- |
| Range (nT) | X sensor | Y sensor | Z sensor |
| R0 32 | 1.005167 | 1.005515 | 1.009559 |
| R1 256 | 1.008589 | 0.998337 | 1.006285 |

Table VI lists the sensitivity of each axis of the VHM, normalized by the nominal maximum field value divided by the maximum number of bits, for each of its two ranges. The digital output from the SHM consists of the number of cycles in an interval of 0.997126 sec and is stored in a register before being transferred to the DPU. The equivalent frequency is then converted to field strength by using the gyromagnetic ratio.

### 4.2. IN-FLIGHT CALIBRATION

For the vector magnetometers, conversion of raw data to magnetic field values is generally achieved by applying an offset and a gain (nT/bit) to the raw data. Additional corrections have to be applied for the sensor alignment and temperature dependencies. Ground calibration provides initial values for these parameters which will vary after launch. In particular, the stray spacecraft field adds to the intrinsic sensor offsets. Further, the alignment of the sensors with respect to the spacecraft cannot be established until after the magnetometer boom is deployed. Various means are available to re-establish the calibration of the instrument after launch.

The built-in IFC functions, described earlier provide a check of the sensor gains. Changes in alignments, both between sensor axes and with respect to the spacecraft axes can be detected by the use of SCAS. Since the alignment of the SCAS coils with respect to the spacecraft are known (measured before launch) and the alignment of the spacecraft axes with respect to an inertial reference system are known, the relationship of the sensor outputs to the inertial reference system can be established. This relationship was also cross-checked by operation of the sensors in the well known Earth's field during flyby. It is likely that the orientation of the sensors on the boom may change slightly after events such as spacecraft manoeuvres or as the thermal environment changes with distance from the sun. To counter this, periodic SCAS alignment checks are planned for the mission, starting during the Science cruise phase. The approximate SCAS fields (zero to peak) expected to be seen at the sensors are, for the FGM, $X = 25$ nT, $Y = 15$ nT and, for the VHM, $X = 2.25$ nT, $Y = 2$ nT ($X$ and $Y$ are spacecraft axes). The periodic change in direction of the fields will make them distinguishable from the ambient external field and spacecraft field.
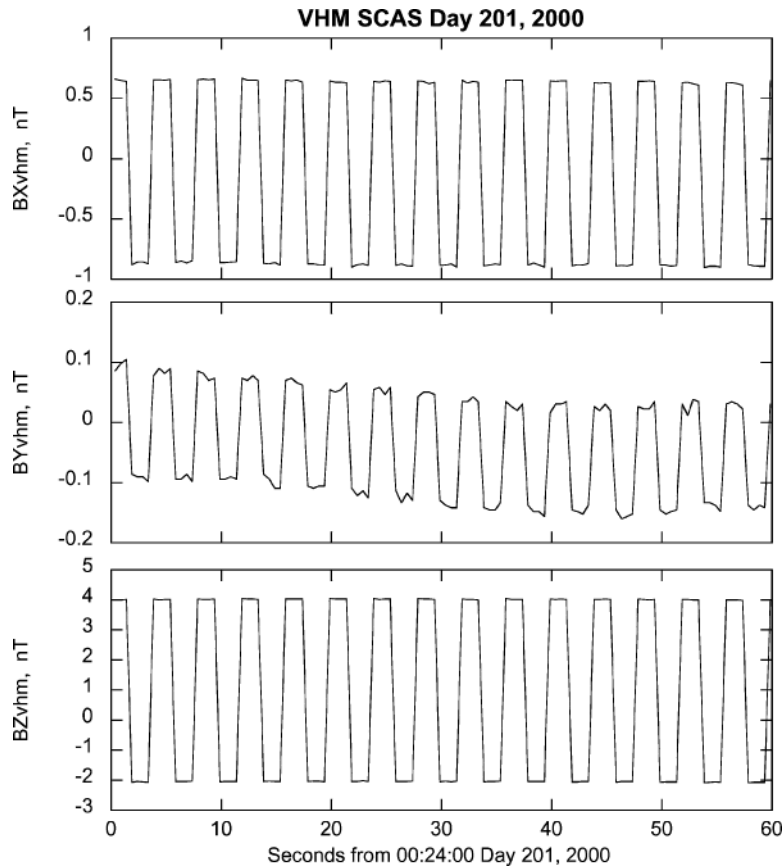
*Figure 12.* VHM data taken during the SCAS operation of Day 201, 2000.

SCAS was operated three times after boom deployment near Earth in August 1999 and twice more during the following year. Figure 12 shows an example of VHM data taken when the SCAS $X$ coil was on. The data are in VHM sensor coordinates (S/C $+ X =$ VHM $- Z$ and S/C $+ Y =$ VHM $+ X$). The time resolution is 8 VHM vectors/second.

The SCAS signals are fairly easily estimated, since their peak to peak values are not affected by the sensors' zero levels, and the operation interval includes a large enough number of 4-sec cycles so that the effects due to ambient fields are negligible. The directions of the SCAS fields at both sensors are consistent within $0.1°$ for all the operation intervals analysed, so the orientation of the sensors has not changed more than this amount over the 1 year from August 1999 through July 2000. Comparison with the predicted SCAS fields at the sensors indicate that the FGM is within $0.3°$ of alignment with the spacecraft axes and the VHM is within $1°$.

Having two independent measurements of the local field at any one time (FGM/VHM or FGM/SHM) provides possibilities for cross-calibration between

sensors. In particular, joint operation of the SHM and FGM (scalar/vector mode), for example during Earth flyby, allow the absolute measurements of the scalar sensor to be used to re-calibrate the FGM, see next section. This is done by least squares fitting of the FGM vector measurements to the scalar field measurements, a technique that has been used on previous missions such as MAGSAT (Langel *et al.*, 1981).

Dual sensor measurements also allow estimates of changes in the spacecraft field to be made. The spacecraft field may vary in-flight due to onboard configuration changes. As the mission progresses we expect to be able to establish a rough correspondence between the spacecraft configuration and spacecraft field which will help in subsequent data analysis. The instrument checkout period (see Section 8.3) provided an opportunity for this since the magnetometer stayed on as each instrument performed its checkout operations. Rotation of the spacecraft (around one axis followed by another) allows an estimate of the offsets (sensor plus spacecraft field) to be made. This is because the detected field component due to the ambient external field will be seen to rotate and that due to sensor offsets and spacecraft field will remain static (in the sensor frame of reference). Using thrusters, the spacecraft is capable of rolling at approximately 0.4°/sec. We plan periodic calibration sessions (of 30 rolls about the Z axis followed by the same about X) during science cruise (once per month) and tour (at each apoapsis). While in the solar wind, offsets (sensor and spacecraft) can also be estimated using a variance technique developed by Davis and Smith (1968), Belcher (1973) and Hedgecock (1975) and used on many previous missions. This technique is based on the fact that interplanetary field fluctuations tend to be transverse to the average direction of the field and conserve the field magnitude. Solar wind observations are possible during science cruise and during those parts of the tour when the orbit leaves the Saturn magnetosphere.

## 4.3. CALIBRATION FROM EARTH SWINGBY

Just prior to Earth swingby, the magnetometer boom was deployed. Deployment was not allowed within 0.85 AU of the Sun, since the boom might have lost structural integrity if too hot. It could also not be deployed until after the trajectory correction manoeuvre (TCM) which optimised the spacecraft trajectory for Earth flyby, due to the additional attitude control uncertainties during TCM introduced by the 11 meter boom. Both the instrument and SCAS were operated during, and immediately after, deployment. This allowed the deployment to be monitored, the spacecraft field to be measured as the separation increased between the sensors and the spacecraft and the post-deployment sensor alignment to be assessed. This was the first of three SCAS operations which took place during the flyby period. The second took place during the flyby itself and the third shortly afterwards. The sensor alignments were checked after deployment, as discussed in the previous section. A combination of vector/vector and vector/scalar modes were used for these activities.
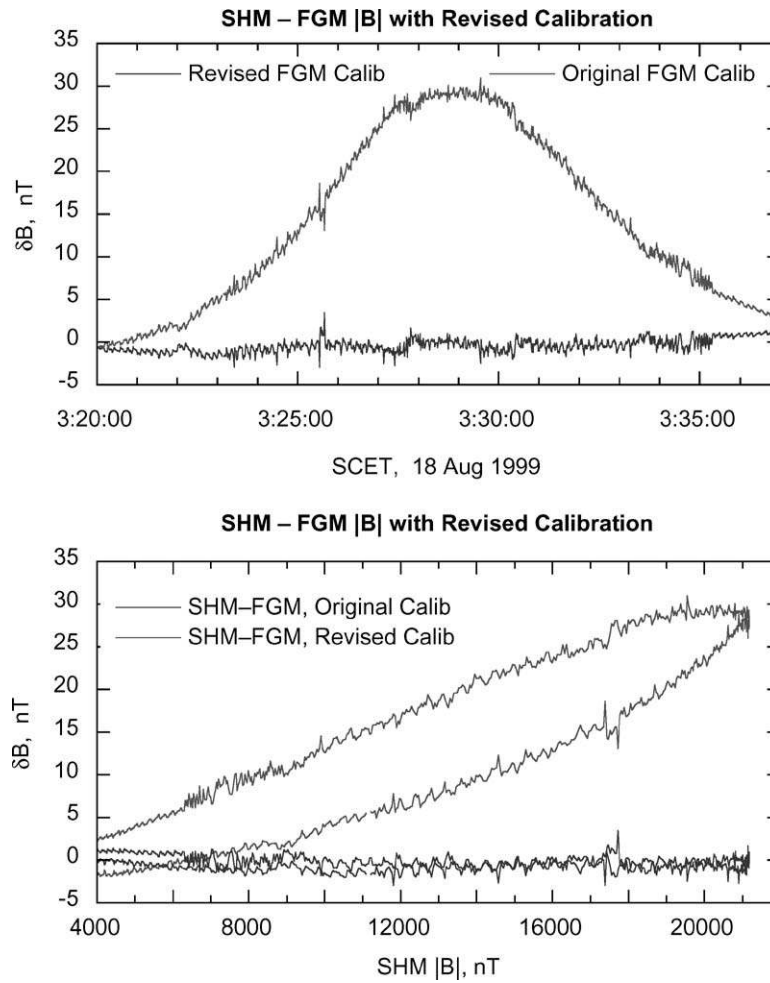
*Figure 13.* SHM − FGM (|B|) differences with original and revised calibrations plotted as a function of time (*top*) and |*B*| (*bottom*).

The trajectory during Earth swingby can be seen in Section 9.2, Figure 19. The high resolution data taken during the flyby then provided an important calibration opportunity for comparing the SHM measurements with the well known Earth field (Smith *et al.*, 2002) and also with the magnitudes derived from the FGM vector measurements. The difference between SHM and FGM |B| reached 30 nT at the peak of 21,200 nT, when the FGM sensor was in its highest range (R3). Adjusting the elements in the FGM R3 calibration matrix that depends upon the non-orthogonality of the FGM sensor's axes reduced the difference to less than 2 nT over the 17-min interval during which |B| varied from 4,000 to 21,200 nT (Figure 13). Using the adjusted calibration matrix also resulted in a significant
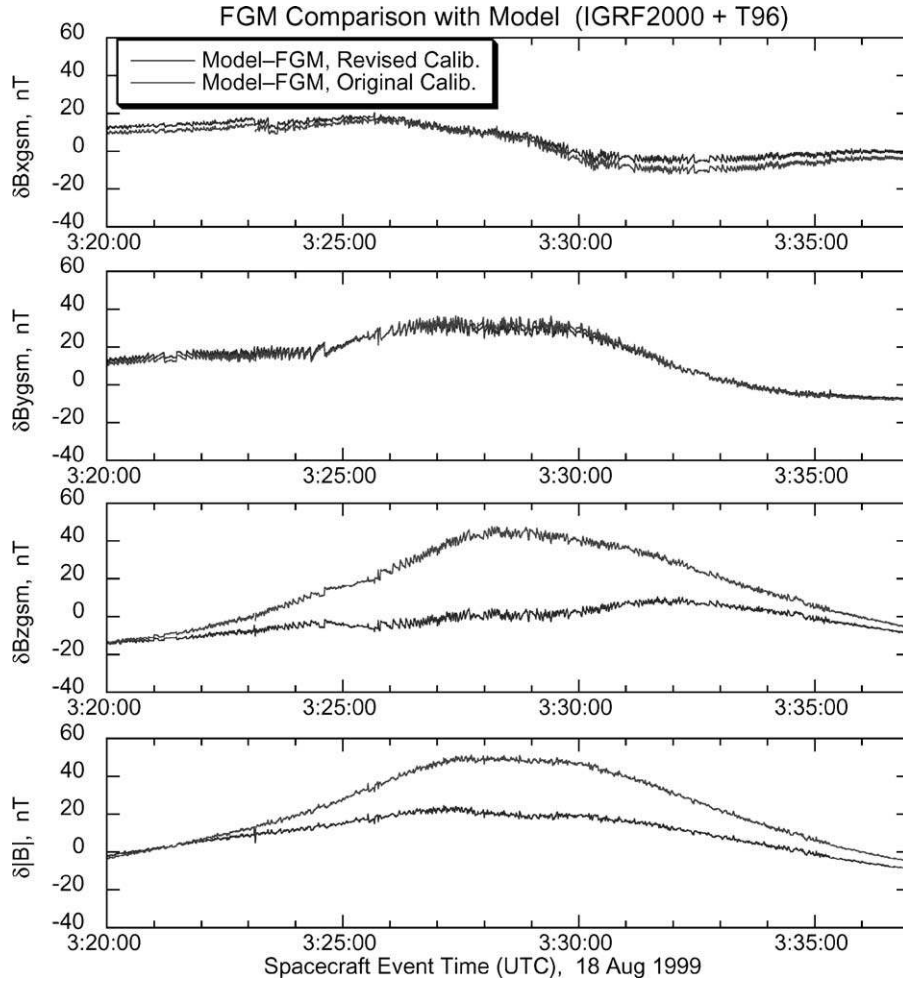
*Figure 14.* Differences of FGM components and magnitude from field model (IGRF2000 + T96), with revised and original FGM calibrations.

decrease of the residuals of FGM vector components and magnitude from the Earth field model (Figure 14). This adjustment is a good example showing how the SHM data can be used to improve the FGM calibration in-flight.

The method used to calculate the adjustments to the calibration matrix was to minimize $(|Af_i| - s_i)^2$ with respect to the elements $a_{21,}$ $a_{31}$ and $a_{32}$ of the matrix A. The diagonal elements of $A$ are set equal to the $X$, $Y$, $Z$ ground calibration sensitivities and the upper triangular elements are zero. Each SHM measurement is indicated by $s_i$ and $f_i$ denotes the FGM average vector corresponding to the interval of the SHM measurement. Values of $a_{21}$, $a_{31}$, and $a_{32}$ from ground calibration were $-0.00005$, $0.00135$, and $-0.0061$, respectively; adjusted values are $0.0022$, $-0.00115$, and $-0.0053$. The adjustments represent changes in the *XY* orthogonality angle of $0.13°$, the *XZ* angle of $0.14°$, and the YZ angle of $0.05°$.

The SHM mode was exercised between 4.0 and $1.17R_E$ both inbound and outbound. The measurements were compared with the Earth's internal field using the International Geomagnetic Reference Field (IGRF 2000). The differences, representing the disturbance field caused by external currents during an on-going magnetic storm, were compared with two models, the Tsyganenko 96 model (available on the NSSDC web site) and the model derived from observations by the POLAR spacecraft (Tsyganenko *et al*., 1999). Better agreement was obtained with the POLAR model although small adjustments to the model parameters were necessary in order to arrive at a closer agreement (within a few nT). Since the Disturbance field contributes mainly to the low degree spherical harmonics describing the internal field, a theorem was developed that allowed a comparison between the higher degree moments of the model and the SHM measurements after removing the low degree terms and the Disturbance field. A close correspondence was then found demonstrating the absolute accuracy of the SHM measurements at the very high level that was anticipated.

## 5.  Spacecraft Magnetic Cleanliness

Due to the complex nature of the Cassini spacecraft the potential for magnetic contamination of the FGM and V/SHM magnetic field data were quite high. Since the goal of achieving a maximum allowable spacecraft magnetic field of 0.2 nT at the V/SHM location would be compromised by this, a magnetic cleanliness program was initiated by the Cassini project team to ensure that the goal would be met. To oversee this program a Magnetics Control Review Board (MCRB) was established, consisting of magnetometer team members as well as members of the Electromagnetics Compatibility Group at JPL. The actions and results which arose from the MCRB are described in detail in Narvaez (2003).

A model of the spacecraft field was developed by the MCRB. A semilogplot of the predicted spacecraft field along the magnetometer boom (Figure 15) provides an indication of the inverse cube fall of the spacecraft field and shows the expected $Y$ field at the position of the two sensors after boom deployment.

A comparison of the VHM and FGM predicted spacecraft fields, following the Huygens probe deplyment, are made in the polar plot in Figure 16. The inverse cube fall-off relationship between the spacecraft fields at the FGM and V/SHM locations are shown. Note also the nearly dipolar shape of both fields at the two locations. Magnetic field measurements will be taken during the deployment of the Huygens probe in December 2004. This will allow the changing spacecraft field from before to after probe deployment to be measured and comparisons to be made with predictions.

The Cassini magnetics control program has been very successful. Each Cassini spacecraft subsystem has made the significant contributions which were necessary to achieve the goals set out by the MCRB. The resulting efforts have paid off for the
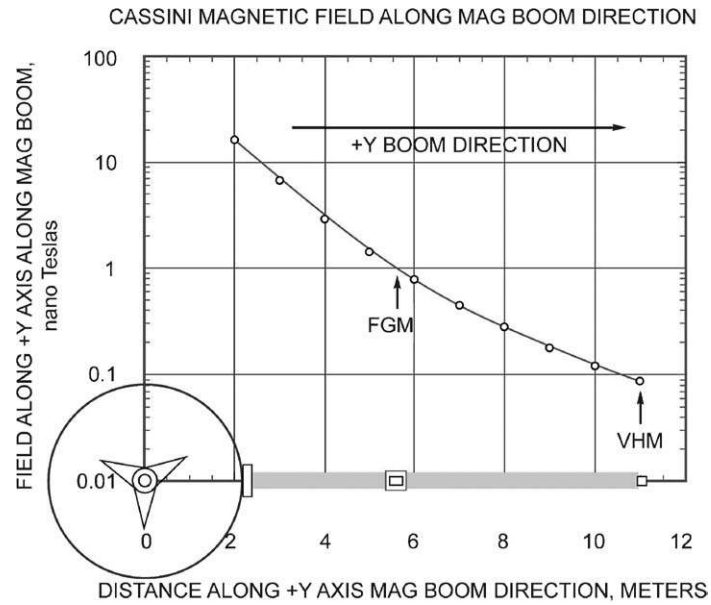
CASSINI MAGNETIC FIELD ALONG MAG BOOM DIRECTION



*Figure 15.* Cassini magnetic field along MAG boom direction.

CASSINI S/C MAGNETIC FIELD POST HUYGENS PROBE DEPLOYMENT
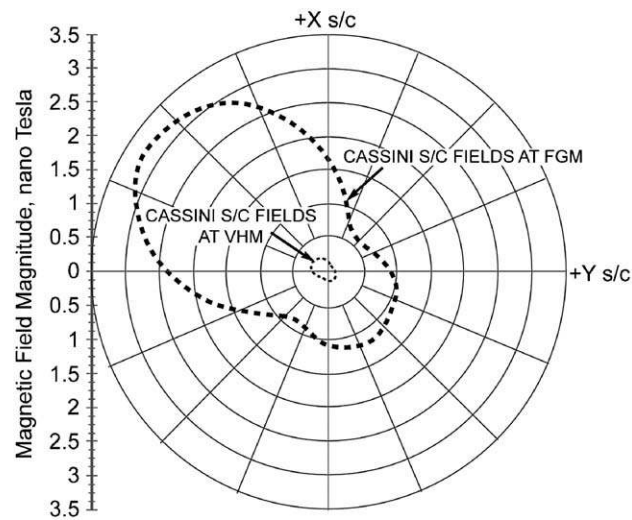AT 5.18 METERS (FGM LOCATION) AND 11.015 METERS (VHM LOCATION)



*Figure 16.* Cassini spacecraft field after Huygens deployment.

science aims of the mission, since if no magnetic cleanliness had been instituted for the Cassini program, the spacecraft fields would have been quite high and variable. The science goals of the magnetometer and other fields and particles instruments would have suffered (see for example the discussion in Section 2.1.1 on the interior of Saturn).

## 6. Instrument Modes and Control

Due to both the large amount of cross-strapped instrument hardware redundancy and the extensive software functionality built into the DPU, numerous operating states can be defined for the instrument. However, a small set of operational modes have been defined which represent the instrument configuration for normal operations: Off, Sleep, Maintenance, Vector/Vector and Vector/Scalar. Figure 17 shows the allowed mode transitions. The modes are further described below:

*Off mode*: In this mode the DPU and instruments are unpowered with the exception of the heater control electronics and sensor heaters. Power is required for the heaters throughout the mission, irrespective of the powered state of the instrument itself. Thus, whenever the instrument is not operating it will be in this mode. No telemetry data are generated by the instrument, and sensor temperatures are available using thermistor data which is processed by the spacecraft. If both heaters were fully powered, the average power consumption would be 3.42 W.

*Sleep mode*: This mode was requested for each instrument by the Cassini project as a minimum power, minimum data rate state that the instrument can be commanded into by single command. Increases in instrument power/data rate are not
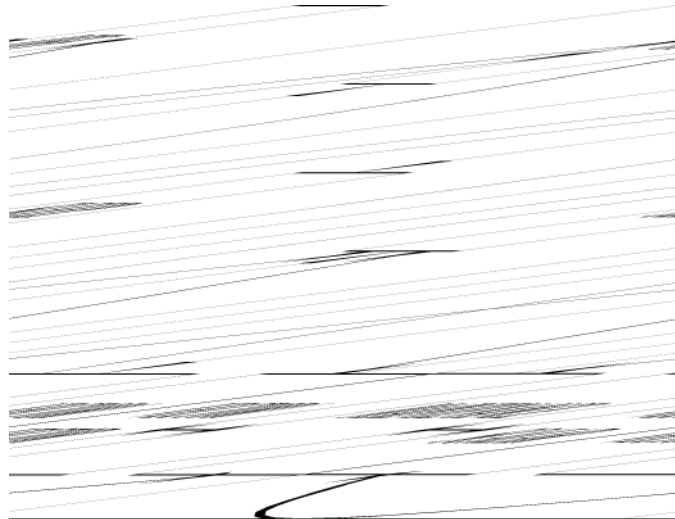


*Figure 17.* Allowed instrument operational mode transitions.

allowed until the instrument is first set active again and commands that could do so must be rejected by the instrument. Spacecraft operational modes have been defined where a particular subset of instruments have priority, the others being in sleep mode. Transition from one spacecraft mode to another can be achieved very quickly and easily since all instruments are still powered. The DPU is powered and running and will block commands to activate other parts of the instrument. Only housekeeping packets are generated; they will normally be collected by the CDS at a rate of one packet per 64 s. The average power consumption is 7.50 W (given in Table IV) and includes heater power.

*Maintenance mode*: During long cruise intervals with the instruments off periodic operation of the V/SHM sensor is needed to maintain the health of the helium cell. In this mode both the DPU and VHM are powered. The DPU prepares science and housekeeping packets but only the housekeeping packets are picked up by the CDS. The packet collection rate is 1 packet per 128 s. Average power consumption is 11.31 W (including heaters).

*Vector/Vector mode*: This mode is used for magnetic field observations in low ambient fields, <256 nT. Both FGM and VHM are operating, providing vector measurements of the field. This permits intercalibration of the sensors which is useful in pinpointing possible changes in the spacecraft field. In normal operations, science packets are collected every 4 sec, housekeeping packets every 64 sec. The average power consumption, including heaters, is 11.31 W.

*Vector/Scalar mode*: Magnetic field observations in high ambient fields, > 256 nT, will be made in this mode. Here the FGM and SHM are operating together. Packet rates are normally the same as those for vector/vector mode, VHM vectors being replaced by SHM scalar values. Average power consumption (including heaters) is 12.63 W.

Most of the commandable functions of the instrument are referred to either directly or indirectly in other sections of this paper. A summary of these functions is provided in Table VII with an indication of their planned usage for the mission shown.

### 7. Onboard Data Processing

The DPU collects sensor science and housekeeping data from the ADC. The FGM science data collection rate is commandable from 16 to 500 vectors/sec, VHM data are collected at a fixed ratio of one sixteenth of the FGM rate. The normal collection rate is 64 FGM vectors/sec. An SHM scalar word is collected once per second. In most operational modes, sensor data are collected at a higher rate than they can be downlinked in telemetry, or may be collected when no telemetry downlink is available. The DPU is able to average the collected data until downlink is available. Two averaging schemes have been implemented, a simple fixed window average where consecutive sets of data are averaged down to a single value, and a running average with a commandable averaging window size. These schemes adapt

TABLE VII

The main commandable functions of the instrument

| FUNCTION | USAGE |
|---|---|
| Heater electronics on/off | Always On |
| Power supply and processor selection | Redundant units only used after failure of primary ones |
| BIU control | Not needed for normal operations |
| Sleep/active state selection | Spacecraft operations mode control |
| Latch up detector and watchdog control | Not needed for normal operations |
| PROM/RAM software select | Not needed for normal operations |
| Software control (reset, registers, tables, parameters etc.) | Not needed for normal operations |
| Science data sampling rate and averaging selection | Science observation dependant |
| Telemetry packet content selection | Fixed for normal operations |
| Snapshot data control | Science observation dependant |
| ADC control/test | Not needed for normal operations |
| FGM, VHM and SHM control | Science observation dependant |
| Initiate Macro commands | Used for observations during tour |
| Memory load/dump/test | Not needed for normal operations |

automatically to the data rates applied by the spacecraft. It is also possible to store and downlink sets of unaveraged data (i.e., sets of data sampled at the best achievable time resolution). Such data are called snapshot data and would be used to sample discrete magnetospheric events. Snapshot data collection can be triggered by command or by built-in trigger algorithms. Several algorithms have been implemented to detect changes in magnitude of the field vector or vector component, changes in field direction, changes in the variance of the field vector or vector component. Up to four algorithms with individually assigned priorities for telemetry readout can be run in parallel and algorithm control parameters are commandable. The snapshot data are stored in one of two areas; in one half of the Hi-Rel 128KB RAM for high reliability but short coverage data and in the commercial 16MB RAM for extended coverage. At a sampling rate of 64 vectors/sec, up to 170 sec worth of data can be stored in the Hi-Rel RAM or 12 h of data in the commercial RAM. Up to 33 snapshot events can be stored at any one time.

Cassini uses the international packet telemetry standard. The DPU generates two types of telemetry packets, housekeeping and science. These packets are of fixed length, 192 bytes housekeeping and 988 bytes science. The generation rate of the packets is modified according to the spacecraft telemetry mode. For normal operations, a science packet is generated every 4 sec and a housekeeping packet every 64 sec, leading to a downlink data rate of 2000 bits/sec. Science packets also

contain a housekeeping data set but the bulk of the packet data area is set aside for FGM, VHM and SHM science data. Again by command, the science data area can be used for special data requests; whereby the science data are replaced by memory readout, ADC noise test or ADC turbo test data. A portion of the packet data area is set aside for the downlink of subcommutated snapshot data and snapshotting status, such as selected algorithms, trigger status and statistics of events occupying the snapshot memory.

The amount of housekeeping data exceeds the size of a housekeeping packet so some data are subcommutated i.e., the full data set is split up and a portion of it put in each packet. The housekeeping packet contains analogue and digital housekeeping data plus the configuration image (the set of all parameters used by the onboard software) and the set of error counters (providing visibility of all tested fault conditions and their frequency). Analogue housekeeping is subcommutated over four packets, the configuration image over 32 packets and the error counters over 64 packets. A portion of the packet, called the maintenance data area, has been set aside for special data requests. By command, the user can select the contents of this area from the following data: configuration image, error counters, high resolution analogue housekeeping and snapshot. Selected data sets which are normally subcommutated can be obtained much more quickly in this way. Optionally, a small set of highly averaged science data, ADC noise test data, ADC turbo test data or memory readout data can be selected by command.

## 8. Launch and Early Cruise Operations

### 8.1. INTRODUCTION

Launched on October 15th 1997, the spacecraft will travel 7 years before Saturn Orbit Insertion (SOI) in July 2004 – this period is called the cruise phase. After arrival it will spend at least 4 years orbiting Saturn and Titan performing science operations – the tour phase. Its trajectory during cruise has included two swingbys around Venus, one around Earth and one past Jupiter. In order to reduce operational costs, spacecraft activities during the cruise phase have been held to the minimum required to maintain the trajectory and the health of the spacecraft and instruments, although some unique science data have also been obtained, see Section 9. Two years before SOI, instrument operations have been increased to include calibration and characterisation in preparation for the tour. Implicit in this concept is a low spacecraft operations team staffing level for the majority of the cruise phase, limiting the possibilities for major science operations. Design of the tour phase operations and the development of key tour phase elements have been deferred to the cruise phase. The magnetometer operations team has followed the same approach. An instrument ground segment has been established which will support the essentially engineering nature of instrument cruise operations and the development of a full science planning and data processing system is being pursued during cruise.

The general mission concept is to avoid real-time commanding where possible and to use the CDS command sequencing capability. However, a near-real-time command capability has been provided which allows commands to be prepared and sent at relatively short notice – from a week to a day in advance.

## 8.2. CRUISE OPERATIONS CONCEPT

All instrument operations for the magnetometer are based at Imperial in line with the distributed operations concept employed by the Cassini project. The operations team is considered a part of the overall spacecraft operations team and is fully responsible for operations. In addition, the team has been assigned responsibility for operations of SCAS. Mission planning is achieved through 'virtual teams' composed of members of the instrument and spacecraft operations teams. The cruise phase is subdivided into approximately 6 month planning periods which are addressed by the Mission Planning Virtual Team (MPVT). Each period is further subdivided into approximately 60 day sequences. As the MPVT completes the planning for one period, these data are handed over to two Sequence Virtual Teams (SVTs) who produce the detailed commands for each sequence. The team provides instrument planning input to the MPVT, reviews planning products, and provides instrument commands to the SVTs.

The main tool for operations support is the Science Operations and Planning Computer (SOPC), provided by the Cassini project and located at Imperial. This workstation is connected via a router and dedicated voice and data lines to the spacecraft monitor and control system at JPL. It is supplied with a suite of software tools to support operations, the same tool as those used by the spacecraft operations team at JPL. The SOPC provides access to instrument and spacecraft telemetry both real-time and that stored in the telemetry database at JPL. Other tools allow the transfer of files containing planning information from the Cassini central database (CDB), allow the generation and transfer of command files to the CDB and give visibility into the detailed spacecraft activity plan and the command sequences prepared for uplink.

Figure 18 is a block diagram of the operations segment at Imperial. Spacecraft and instrument housekeeping and instrument science data are transferred from JPL to the SOPC. The housekeeping data are displayed and stored on the SOPC for instrument health and safety monitoring. The instrument housekeeping and science data are transferred to and stored on the instrument Ground Support Equipment (GSE) for science quicklook data and additional instrument health checks. Instrument command sequences are generated on the PCs and are tested by transfer to the GSE and execution on the Engineering Model (EM) instrument. The error free sequences are then delivered to JPL via the SOPC. Files generated at JPL during the uplink preparation process are checked on the operational PCs using software developed to filter these files for instrument-related information. If required, instrument flight software patches will be produced by the DPU developers, TUB. The patch
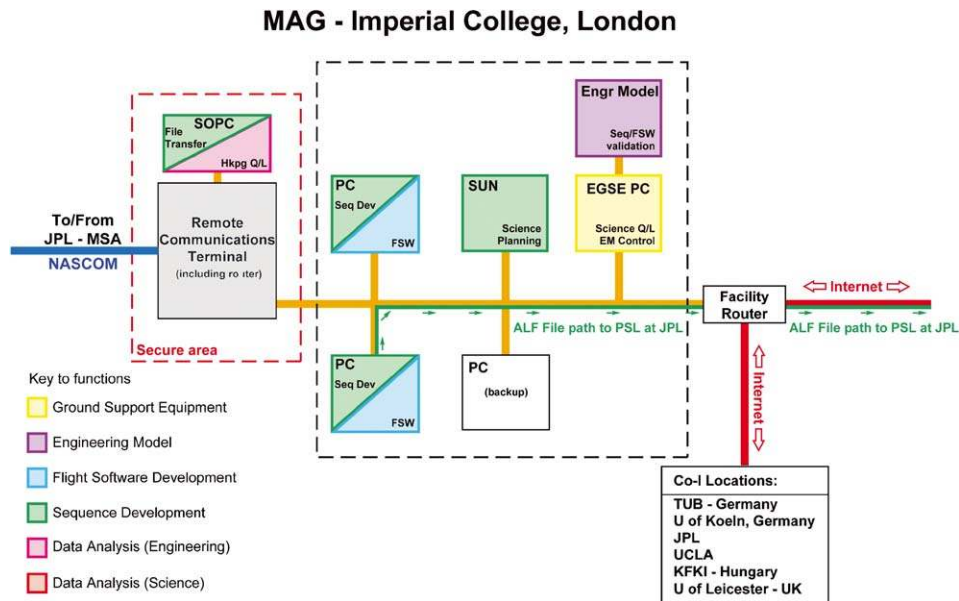
**MAG - Imperial College, London**



*Figure 18.* Operations segment at Imperial College.

files will be transferred to the PCs where they will be converted into the load format needed by JPL and then delivered to the JPL software library. The science planning workstation is used to generate predictions of expected magnetic field strengths and directions as a function of time. These predictions will drive the spacecraft attitude and instrument modes requested during the mission planning process.

Reliability in an operational system is essential. To guard against failures, the operations PCs are triple redundant and the software on the science planning workstation is duplicated on the SOPC. Duplication has also been built into the network interfacing the operational machines.

## 8.3. ACTIVITIES

Instrument operations during cruise are limited to the following: heater activation, sensor temperature monitoring, periodic VHM maintenance, instrument and SCAS checkout, boom deployment, sensor alignment verification during Earth flyby, in-flight calibration. These activities are briefly described below. In addition, quasi-continuous operation usually at low data rate is allowed for cruise science when not impacting other higher priority spacecraft activities. This has included operation during the spacecraft flyby of Jupiter.

Safe non-operating and operating temperature ranges have been defined for both sensors. The sensor temperatures are being monitored regularly since launch to detect trends outside the safe limits. As described in the modes section, heaters

have been provided to help maintain the temperatures within limits. The heaters were activated during the launch sequence, at 75 min after launch. Their function is being monitored by comparing the sensor temperatures with the current drawn by the control electronics.

The VHM sensor must be operated occasionally to maintain the performance of the gas cell. Periodic instrument maintenance (PIM) activities of 2.5 h duration take place approximately every 3 months for the duration of the cruise phase if the VHM is not already powered for cruise science. The instrument is operated in maintenance mode. Only real-time, low rate, housekeeping telemetry is available during PIM.

About 14 months after launch, a period of approximately 25 days was set aside for a comprehensive checkout of each instrument. This was the first opportunity for proper instrument operation since launch. A period of 24 h was allocated for the magnetometer instrument checkout during which all instrument modes and commands were exercised. The magnetometer was then powered for the remainder of the checkout period in order to observe the magnetic signatures of the other instruments (although at this stage the boom was not yet deployed). Checkout of SCAS was also included. The importance of instrument operations during Earth flyby for alignment calibration has been discussed above. In-flight calibration operations will start 2 years before SOI. The activities to be performed have been described earlier in the calibration section.

Boom deployment and instrument calibration and science operations during Earth swingby are discussed elsewhere. More intensive in-flight calibration operations will start 2 years before SOI. The activities to be performed have been described earlier in the calibration section.

## 9. Cruise Science

Cassini was launched on October 15, 1997 at 08:43 GMT. The instrument heaters were successfully activated at 10:08 GMT and within a day the sensor temperatures had stabilised. Due to the long interplanetary cruise trajectory which the spacecraft had to follow in order to make use of numerous planetary gravity assists to place Cassini into Saturn orbit there have been a number of opportunities for cruise science. These consist of interplanetary cruise science, Jupiter flyby science and Earth swingby science and calibration. The analysis of the cruise science data is in its infancy since the team has been concentrating on science planning for the 4-year orbital Cassini tour.

### 9.1. Interplanetary Cruise Science

Continuous taking of fields and particles data began in February 2000, following High Gain Antenna Acquisition. This is very important scientifically since

it will allow interplanetary observations to be made between 2.3–9.5 AU around the time of solar maximum with an advanced payload of instruments. This will enable a multi-point study to be made with distance of the heliospheric magnetic field signatures of large-scale solar wind flow structures such as stream interaction regions and coronal mass ejections (CMEs). In particular, the interplanetary signatures of CMEs have not previously been studied with such comprehensive instrumentation at distances beyond the orbit of Jupiter. In this distance range they are thought to become less and less distinct from the ambient solar wind. These observations by Cassini are being carried out in conjunction with near-Earth spacecraft at 1 AU, with Ulysses between 1.3–5.4 AU and with Voyager beyond 75 AU, the first time that such a joint opportunity has arisen. There are also plans to study waves and turbulence in the solar wind at a much higher time resolution than has previously been possible at these distances (up to 32 vectors/sec).

## 9.2. EARTH SWINGBY

The crucial aspect of this flyby for the instrument was the deployment of the magnetometer boom 4 days before closest approach to the Earth and the acquisition of vector and scalar data in the well known Earth's magnetic field allowing calibration of the instrument. This aspect of the flyby was discussed in some detail in Section 4.3. Figure 19 shows the spacecraft trajectory during the flyby (from Southwood *et al.*, 2002). Science analysis of the magnetic field data from the flyby has resulted in numerous publications clearly highlighting the instrument's performance in detection of magnetic phenomena in a planetary environment. Due to the very high flyby speed ($\sim$16 km/sec) and the high time resolution of the magnetic field observations (32 vectors/sec) significant new information was obtained on a variety of topics including possible evidence of the plasmasphere interchange instability (see Khan *et al.*, 2001; Smith *et al.*, 2001; Southwood *et al.*, 2001; Tsurutani *et al.*, 2001).

## 9.3. JUPITER FLYBY

This unique science opportunity during late 2000, consisted of observations from the Cassini spacecraft while in the upstream solar wind on its approach to Jupiter as well as on the previously unexplored equatorial dusk flank where it made numerous entries into the magnetosheath as well as two brief entries into the flank magnetosphere. In addition during this time the Galileo spacecraft continued its orbital tour of Jupiter and made observations deep inside the inner magnetosphere as Cassini approached in the upstream solar wind and then in turn was out in the solar wind.
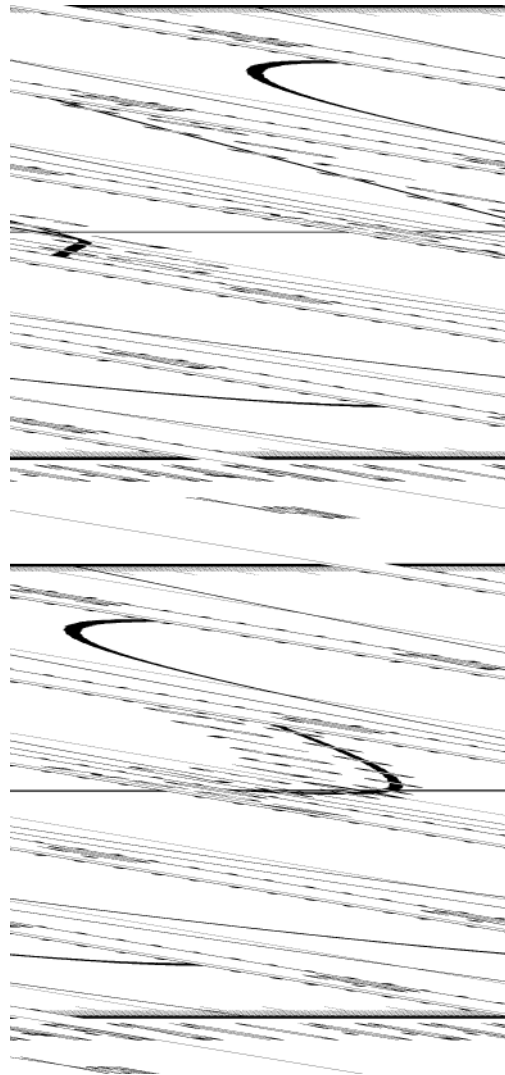
*Figure 19.* Spacecraft trajectory during the Earth swingby in both the (*X*, *Y*) and (*X*, *Z*) GSM planes.

A crucial aspect of these studies is that they will serve as a focal point for illuminating comparative studies of the Jovian and Saturnian magnetospheres. This data is largely unexplored to date since there is no science support in place for Cassini. However, a recent issue of the science journal Nature highlighted some of the science findings from this opportunity. Magnetic field data from the magnetometer onboard Cassini contributed to the findings of three of these papers (as described below). The two spacecraft conjunction at Jupiter in combination with remote sensing observations of the planet by the Earth orbiting Hubble Space Telescope and Chandra Telescope have allowed the effects of the solar wind on

changes within the magnetosphere to be monitored. The magnetosphere of Jupiter and its hectometric radio emissions and aurorae are seen to respond to interplanetary shock waves within the solar wind (Gurnett *et al.*, 2002). The two spacecraft, separated by some 9 million kilometres, encountered the boundary of the magnetosphere while it was contracting in response to an increase in solar wind pressure (Kurth *et al.*, 2002). The presence of both spacecraft proved critical in enabling scientists to prove that the magnetosphere is indeed controlled by the solar wind. In addition a pulsating X-ray hotspot was observed near Jupiter's north pole (Gladstone *et al.*, 2002). This hotspot pulsates every 45 minutes, a periodicity previously observed near Jupiter in radio and energetic electron bursts. It does not appear to be influenced by any changes in the solar wind but by some as yet unknown factor inside the magnetosphere.

The three main topics which the magnetometer data set will be used to address are:

*Solar-wind Jupiter magnetospheric interaction*

We know that the dynamics of the rotationally driven Jovian magnetosphere are very different from that of the Earth's solar wind driven one, where at Jupiter the fast rotation imposed by the planet is communicated throughout the magnetosphere by the magnetic field. The important question is how do changes in the solar wind effect the internal magnetic activity within the magnetosphere?

*Dynamics of the outer Jovian environment*

How do the outer boundaries of the Jovian environment (the bow shock and magnetopause), respond to changes in the interplanetary medium and how quickly can these changes occur? How are these changes then fed into the outer Jovian environment? Two point measurements of these boundaries made by Cassini and Galileo during this period will allow some resolution of the dynamics of the system as well as the shape of the boundaries which is thought to be much less rigid than originally modelled. Some initial analysis of numerous occasions of mirror mode activity within the Cassini magnetosheath (André *et al.*, 2002) shows that the Cassini Jupiter flyby allows tracking of the mirror instability along flow lines down to the distant jovian magnetosheath, as yet unexplored by previous missions. The most distant observations of mirror mode activity were measured hundreds of radii downstream in the post-dusk magnetosheath where either isolated or very long sequence of magnetic bi-stated dropouts appeared.

*Solar wind structure*

Dual spacecraft measurements have not been made before of the interplanetary medium in the vicinity of Jupiter. Observations of similar but evolving solar wind structures at the two spacecraft have been observed separated by radial distance of some $750\,R_J$. Understanding the similarities and differences between such structures will allow us to gain a better understanding of the evolution of structure within the solar wind at 5 AU.

## Acknowledgements

## References

Acuna, M. H., Connerney, J. E. P., and Ness, N. F.: 1983, *J. Geophys. Res.* **88**, 8771.

André, N., Erdos, G., and Dougherty, M. K.: 2002, *Geophys. Res. Letters*, in press.

Balogh, A., *et al.*: 1992, *Astron. Astrophys. Suppl. Ser.* **92**, 221.

Behannon, K. W., Connerney, J. E. P., and Ness, N. F.: 1981, *Nature* **292**, 753.

Belcher, J. W.: 1973, *J. Geophys. Res.* **78**, 6480.

Ben-Jaffel, L., Leers, V., and Sandel, B.: 1995, *Science* **269**, 951.

Bhardwaj, A. and Gladstone, G. R.: 1982, *Rev. Geophys.* **38**, 295.

Blanc, M., *et al.*: 2002, *Space Sci. Rev.*, in print.

Bunce, E. J. and Cowley, S. W. H.: 2002, *Ann. Geophysica*, submitted.

Carbary, J. F. and Krimigis, S. M.: 1982, *Geophys. Res. Lett.* **9**, 1073.

Caudal, G: 1986, *J. Geophys. Res.* **91**, 4201.

Connerney, J. E. P., Ness, N. F., and Acuna, M. H.: 1982, *Nature* **298**, 44.

Connerney, J. E. P., Acuna, M. H., and Ness, N. F.: 1983, *J. Geophys. Res.* **88**, 8779.

Connerney, J. E. P.: 1993, *J. Geophys. Res.* **98**, 18659.

Cramm, R., Glassmeier, K.-H., Stellmacher, M., and Othmer, C.: 1998, *J. Geophys. Res.* **103**, 11951.

Davis, L. Jr. and Smith, E. J.: 1968, *Trans. AGU* **49**, 257.

Davis, L. and Smith, E. J.: 1986, *J. Geophys. Res.* **91**, 1373.

Davis, L. and Smith, E. J.: 1990, *J. Geophys. Res.* **95**, 15257.

Dougherty, M. K., Southwood, D. J., Balogh, A., and Smith, E. J.: 1993, *Planet. Space Sci.* **41**, 291.

Dougherty, M. K. and Southwood, D. J.: 1993, *Adv. Space Res.* **13**, 10305.

Dougherty, M. K., Southwood, D. J., and Lachin, A.: 1997, *Adv. Space Res.* **20**, 215.

Dougherty, M. K., Dunlop, M. W., Prange, R., and Rego, D.: 1998, *Planet. Space Sci.* **46**, 531.

Elphic, R. C. and Russell, C. T.: 1978, *Geophys. Res. Lett.* **5**, 211.

Espinosa, S. A. and Dougherty, M. K.: 2000, *Geophys. Res. Lett.* **27**, 2785

Eviatar, A., Siscoe, G. L., Scudder, J. D., Sittler, E. C., and Sullivan, J. D.: 1982, *J. Geophys. Res.* **87**, 8091.

Giampieri, G. and Dougherty, M. K.: 2002, *Geophys. Res. Lett.*, submitted.

Gladstone, G. R., Waite, J. H., Grodent, Jr, D., Lewis, W. S., Crary, F. J., Elsner, R. S., Weisskopf, M. C., Majeed, T., Jahn, J.-M., Bhardwaj, A., Clarke, J. T., Young, D. T., Dougherty, M. K., Espinosa, S. A., and Cravens, T. E.: 2002, *Nature* **415**, 1000.

Goertz, C.: 1983, *Geophys. Res. Lett.* **10**, 455.

Grun, E., Goertz, C. K., Morfill, G. E., and Havnes, O.: 1992, *Icarus* **99**, 191.

Gurnett, D. A., Kurth, W. S., Hospodarsky, G. B., Persoon, A. M., Zarka, P., Lecacheux, A., Bolton, S. J., Desch, M. D., Farrell, W. M., Kaiser, M. L., Ladreiter, H.-P., Rucker, H. O., Galopeau, P., Louarn, P., Young, D. T., Pryor, W. R., and Dougherty, M. K.: 2002, *Nature* **415**, 985.

Haynes, P. L., Balogh, A., Dougherty, M. K., Southwood, D. J., Fazakerley, A., and Smith, E. J.: 1994, *Geophys.Res. Lett.* **21**, 405.

Hedgecock, P.C: 1975, *Space Sci. Instr.* **1**, 83.

Huddleston, D.E., Strangeway, R. J., Warnecke, J., Russell, C. T., Kivelson, M. G., and Bagenal, F.: 1997, *Geophys. Res. Lett.* **24**, 2143.

Huddleston, D. E., Strangeway, R. J., Warnecke, J., Russell, C. T., and Kivelson, M. G.: 1998, *J. Geophys. Res.* **103**, 19877.

Huddleston, D. E., Strangeway, R. J., Blanco-Cano, X., Russell, C. T., Kivelson, M. G., and Khurana, K. K.: 1999, *J. Geophys. Res.* **104**, 17479.

Kabin, K., Israelevich, P. L., Ershkovich, A., Neubauer, F. M., Gombosi, T. I., de Zeeuw, D. L., and Powell, K. G.: 2000, *J. Geophys. Res*. **105**, 10761.

Kaiser, M. L., Desch, M. D., Kurth, W. S., Lecacheux, A., Genova, F., Pedersen, B. M., and Evans, D. R.: 1984, *Saturn*, T. Gehrels and M. S. Matthews, eds. (Univ. Arizona Press), 378.

Keller, C. N., Cravens, T. E., and Jan, L.: 1994, *J. Geophys. Res*. **99**, 6511.

Kellock, S., Austin, P., Balogh, A., Gerlach, B., Marquedant, R., Musmann, G., Smith, E., Southwood, D., and Szalai, S.: 1996, *Proc. SPIE*, Denver, Colorado, **2803**, 141.

Khan H., Cowley, S. W. H., Kolesnikova, E., Lester, M., Brittnacher, M. J., Hughes, T. J., Kurth, W. S., McComas, D. J., Newitt, L., Owen, C. J., Reeves, G. D., Singer, H. J., Smith, C. W., Southwood, D. J., and Watermann, J. F.: 2001, *J. Geophys. Res*. **106**, 30141.

Khurana, K. K: 1997, *J. Geophys, Res*. **102**, 11295.

Kivelson, M. G., Khurana, K. K., Walker, R. J., Russell, C. T., Linker, J. A., Southwood, D. J., and Polanskey, C.: 1996a, *Science*, **273**, 337.

Kivelson, M. G., Khurana, K. K., Walker, R. J., Warnecke, J., Russell, C. T., Linker, J. A., Southwood, D. J., and Polanskey, C.: 1996b, *Science* **274**, 396.

Kivelson, M. G., Khurana, K. K., Walker, R. J., Warnecke, J., Russell, C. T., Coroniti, F. V., Polanskey, C., Southwood, D. J. and Schubert, G.: 1996c, *Nature*, **384** 537.

Kivelson, M. G., Khurana, K. K., Coroniti, F. V., Joy, S., Russell, C. T., Walker, R. J., Warnecke, J., Bennett, L., and Polanskey, C.: 1997, *Geophys. Res. Lett* **24**, 2155.

Kivelson, M. G., Khurana, K. K., Russell, C. T., Volwerk, M., Walker, R. J., and Zimmer, C.: 2000, *Science*, **289**, 1340.

Kivelson, M. G., Bagenal, F., Neubauer, F. M., Paranicas, C., and Saur, J.: 2002,*Jupiter*, F. Bagenal, ed., (Cambridge Univ. Press), in press.

Kurth, W. S., Gurnett, D. A., Hospodarsky, G. B., Farrell, W. M., Roux, A., Dougherty, M. K., Joy, S. P., Kivelson, M. G., Walker, R. J., Crary, F. J., and Alexander, C. J.: 2002, *Nature* **415**, 991.

Langel, R., Berbert, J., Jennings, T., Horner, R.: 1981, NASA/GSFC TM 82160.

Leamon, R. L., Dougherty, M. K., Southwood, D. J., and Haynes, P. L.: 1995, *J. Geophys. Res*. **100**, 1829.

Lepping, R. P., Desch, M. D., Klein, L. W., Sittler, E. C., Sullivan, J. D., Kurth W. S., and Behannon, K. W.: 1983, *J. Geophys. Res*. **88**, 8801.

Maurice, S. and Engle, I.: 1995, *J. Geophys. Res*. **100**, 17143.

McNutt, R. L., Jr.:1983, *Adv. Space Res*. **3**, 55.

Narvaez, P; 2003, *Space Sci.Rev*. this volume.

Neubauer, F. M., D. A. Gurnett, J. D. Scudder and R. E. Hartle: 1984, in Saturn, eds T. Gehrels and M. S. Matthews (Univ. Arizona Press), 760.

Neubauer, F. M.: 1999, *J. Geophys. Res*. **104**, 28671.

Richardson, J. D.: 1986, *J. Geophys. Res*. **91**, 1381.

Southwood, D. J., Dougherty, M. K., Leamon, R. J., and Haynes, P. L.: 1995, *Adv. Space Res*. **16**, 4177.

Southwood, D. J., Dougherty, M. K., Balogh, A., Cowley, S. W. H., Smith, E. J., Tsurutani, B. T.,Russell, C. T., Siscoe, G. L., Erdos, G., Glassmeier, K.-H., Gleim, F., and Neubauer, F. M.: 2001, *J. Geophys. Res*., 30109.

Smith, E. J., Davis, L., Jones, Jr., D. E., Coleman, P. J., Colburn, Jr., D. S., Dyal, P., and Sonnet, C. P.: 1980a, *Science* **207**, 407.

Smith, E. J., Davis, L., Jones, Jr., D. E., Coleman, P. J., Colburn, Jr., D. S., Dyal, P., and Sonnet, C. P.: 1980b, *J. Geophys. Res*. **85**, 5655.

Smith, E. J., Dougherty, M. K., Russell, C. T., and Southwood, D. J.: 2001, *J. Geophys. Res*. 30129.

Stevenson, D. J: 1980, *Science* **208**, 746.

Thompson, P., Dougherty, M. K., Southwood, D. J.: 1995, *Planet. Space Sci*. **43**, 625.

Tsurutani, B. T., Smith, E. J., Anderson, R. R., Ogilvie, K. W., Scudder, J. D., Baker, D. N., and Bame, S. J.: 1982*, J. Geophys. Res*. **87**, 6060.

Tsurutani, B. T., Southwood, D. J., Smith, E. J., and Balogh, A.:1993, *J. Geophys. Res*. **98**, 21203.

Tsurutani, B. T., Southwood, D. J., Dougherty, M. K., Smith, E. J., Burton, M. E., Glassmeier, K.-H., Neubauer, F. M., Arballo, J. K., Galvan, C., Zhou, X.-Y., and Chao, J. K.: 2001, *J. Geophys. Res*., 30223.

Tsyganenko, N. A: 1989, *Planet. Space Sci*. **37**, 5.

Tsyganenko, N. A. and Peredo, M.: 1994, *J. Geophys. Res*. **99**, 199.

Tsyganenko, N. A., Le, G., Russell, C. T., and Iyemori, T.: 1999, *J. Geophys. Res*. **104**, 10275.